International Tables for Crystallography (2016). Vol. A, Chapter 1.6, pp. 107–131.

1.6. Methods of space-group determination

U. Shmueli, H. D. Flack and J. C. H. Spence

1.6.1. Overview

This chapter describes and discusses several methods of symmetry determination of single-domain crystals. A detailed presentation of symmetry determination from diffraction data is given in Section 1.6.2.1, followed by a brief discussion of intensity statistics, ideal as well as non-ideal, with an application of the latter to real intensity data from a $P\overline{1}$ crystal structure in Section 1.6.2.2. Several methods of retrieving symmetry information from a solved crystal structure are then discussed (Section 1.6.2.3). This is followed by a discussion of chemical and physical restrictions on space-group symmetry (Section 1.6.2.4), including some aids in symmetry determination, and by a brief section on pitfalls in space-group determination (Section 1.6.2.5).

The following two sections deal with reflection conditions. Section 1.6.3 presents the theoretical background of conditions for possible general reflections and their corresponding derivation. A brief discussion of special reflection conditions is included. Section 1.6.4 presents an extensive tabulation of general reflection conditions and possible space groups.

Other methods of space-group determination are presented in Section 1.6.5. Section 1.6.5.1 deals with an account of methods of space-group determination based on resonant (also termed 'anomalous') scattering. Section 1.6.5.2 is a brief description of approaches to space-group determination in macromolecular crystallography. Section 1.6.5.3 deals with corresponding approaches in powder-diffraction methods.

The chapter concludes with a description and illustration of symmetry determination based on electron-diffraction methods (Section 1.6.6), and principally focuses on convergent-beam electron diffraction.

This chapter deals only with single crystals. A supplement (Flack, 2015) deals with twinned crystals and those displaying a specialized metric.

1.6.2. Symmetry determination from single-crystal studies

By U. Shmueli and H. D. Flack

1.6.2.1. Symmetry information from the diffraction pattern

The extraction of symmetry information from the diffraction pattern takes place in three stages.

In the first stage, the unit-cell dimensions are determined and analyzed in order to establish to which Bravais lattice the crystal belongs. A conventional choice of lattice basis (coordinate system) may then be chosen. The determination of the Bravais lattice[1] of the crystal is achieved by the process of cell reduction, in which the lattice is first described by a basis leading to a primitive unit cell, and then linear combinations of the unit-cell vectors are taken to reduce the metric tensor (and the cell dimensions) to a standard form. From the relationships amongst the elements of the metric tensor, one obtains the Bravais lattice, together with a conventional choice of the unit cell, with the aid of standard tables. A detailed description of cell reduction is given in Chapter 3.1 of this volume and in Part 9 of earlier editions (*e.g.* Burzlaff *et al.*, 2002). An alternative approach (Le Page, 1982) seeks the Bravais lattice directly from the cell dimensions by searching for all the twofold axes present. All these operations are automated in software. Regardless of the technique employed, at the end of the process one obtains an indication of the Bravais lattice and a unit cell in a conventional setting for the crystal system, primitive or centred as appropriate. These are usually good indications which, however, must be confirmed by an examination of the distribution of diffracted intensities as outlined below.

In the second stage, it is the point-group symmetry of the intensities of the Bragg reflections which is determined. We recall that the average reduced intensity of a pair of Friedel opposites (hkl and $\overline{hkl}$) is given by

$$\begin{aligned}|F_{\rm av}(\mathbf{h})|^2 &= \tfrac{1}{2}[|F(\mathbf{h})|^2 + |F(\overline{\mathbf{h}})|^2] \\ &= \sum_{i,j}[(f_i + f_i')(f_j + f_j') + f_i'' f_j'']\cos[2\pi\mathbf{h}(\mathbf{r}_i - \mathbf{r}_j)] \equiv A(\mathbf{h}),\end{aligned} \tag{1.6.2.1}$$

where the atomic scattering factor of atom j, taking into account resonant scattering, is given by

$$\mathbf{f}_j = f_j + f_j' + if_j'',$$

the wavelength-dependent components f_j' and f_j'' being the real and imaginary parts, respectively, of the contribution of atom j to the resonant scattering, $\mathbf{h}$ contains in the (row) matrix (1×3) the diffraction orders (hkl) and $\mathbf{r}_j$ contains in the (column) matrix (3×1) the coordinates (x_j, y_j, z_j) of atom j. The components of the $\mathbf{f}_j$ are assumed to contain implicitly the displacement parameters. Equation (1.6.2.1) can be found *e.g.* in Okaya & Pepinsky (1955), Rossmann & Arnold (2001) and Flack & Shmueli (2007). It follows from (1.6.2.1) that

$$|F_{\rm av}(\mathbf{h})|^2 = |F_{\rm av}(\overline{\mathbf{h}})|^2 \text{ or } A(\mathbf{h}) = A(\overline{\mathbf{h}}),$$

regardless of the contribution of resonant scattering. Hence the averaging introduces a centre of symmetry in the (averaged) diffraction pattern.[2] In fact, working with the average of Friedel opposites, one may determine the Laue group of the diffraction pattern by comparing the intensities of reflections which should be symmetry equivalent under each of the Laue groups. These are the 11 centrosymmetric point groups: $\overline{1}$, $2/m$, mmm, $4/m$, $4/mmm$, $\overline{3}$, $\overline{3}m$, $6/m$, $6/mmm$, $m\overline{3}$ and $m\overline{3}m$. For example, the reflections of which the intensities are to be compared for the Laue group $\overline{3}$ are: hkl, kil, ihl, $\overline{hkl}$, $\overline{kil}$ and $\overline{ihl}$, where $i = -h - k$. An extensive listing of the indices of symmetry-related reflections in all the point groups, including of course the Laue groups, is

[1] The Bravais lattice symbol consists of two characters. The first is the first letter of the name of a crystal family and the second is the centring mode of a conventional unit cell. For details see Tables 3.1.2.1 and 3.1.2.2.

[2] We must mention the well known Friedel's law, which states that $|F(\mathbf{h})|^2 = |F(\overline{\mathbf{h}})|^2$ and which is only a reasonable approximation for noncentrosymmetric crystals if resonant scattering is negligibly small. This law holds well for centrosymmetric crystals, independently of the resonant-scattering contribution.

given in Appendix 1.4.4 of *International Tables for Crystallography* Volume B (Shmueli, 2008).[3] In the past, one used to inspect the diffraction images to see which classes of reflections are symmetry equivalent within experimental and other uncertainty. Nowadays, the whole intensity data set is analyzed by software. The intensities are merged and averaged under each of the 11 Laue groups in various settings (*e.g.* 2/*m* unique axis *b* and unique axis *c*) and orientations (*e.g.* $\bar{3}m1$ and $\bar{3}1m$). For each choice of Laue group and its variant, an $R_{\rm merge}$ factor is calculated as follows:

$$R_{{\rm merge},i} = \frac{\sum_{\mathbf{h}} \sum_{s=1}^{|G|_i} |\langle |F_{\rm av}(\mathbf{h})|^2 \rangle_i - |F_{\rm av}(\mathbf{h}\boldsymbol{W}_{si})|^2|}{|G|_i \sum_{\mathbf{h}} \langle |F_{\rm av}(\mathbf{h})|^2 \rangle_i}, \qquad (1.6.2.2)$$

where $\boldsymbol{W}_{si}$ is the matrix of the *s*th symmetry operation of the *i*th Laue group, $|G_i|$ is the number of symmetry operations in that group, the average in the first term in the numerator and in the denominator ranges over the intensities of the trial Laue group and the outer summations $\sum_{\mathbf{h}}$ range over the *hkl* reflections. Choices with low $R_{{\rm merge},i}$ display the chosen symmetry, whereas for those with high $R_{{\rm merge},i}$ the symmetry is inappropriate. The Laue group of highest symmetry with a low $R_{{\rm merge},i}$ is considered the best indication of the Laue group. Several variants of the above procedure exist in the available software. Whichever of them is used, it is important for the discrimination of the averaging process to choose a strategy of data collection such that the intensities of the greatest possible number of Bragg reflections are measured. In practice, validation of symmetry can often be carried out with a few initial images and the data-collection strategy may be based on this assignment.

In the third stage, the intensities of the Bragg reflections are studied to identify the conditions for systematic absences. Some space groups give rise to zero intensity for certain classes of reflections. These 'zeros' occur in a systematic manner and are commonly called systematic absences (*e.g.* in the *h*0*l* class of reflections, if all rows with *l* odd are absent, then the corresponding reflection condition is *h*0*l*: $l = 2n$). In practice, as implemented in software, statistics are produced on the intensity observations of all possible sets of 'reflections conditions' as given in Chapter 2.3 (*e.g.* in the example above, *h*0*l* reflections are separated into sets with $l = 2n$ and those with $l = 2n + 1$). In one approach, the number of observations in each set having an intensity (I) greater than n standard uncertainties [$u(I)$] [*i.e.* $I/u(I) > n$] is displayed for various values of n. Clearly, if a trial condition for systematic absence has observations with strong or medium intensity [*i.e.* $I/u(I) > 3$], the systematic-absence condition is not fulfilled (*i.e.* the reflections are not systematically absent). If there are no such observations, the condition for systematic absence may be valid and the statistics for smaller values of n need then to be examined. These are more problematic to evaluate, as the set of reflections under examination may have many weak reflections due to structural effects of the crystal or to perturbations of the measurements by other systematic effects. An alternative approach to examining numbers of observations is to compare the mean value, $\langle I/u(I) \rangle$, taken over reflections obeying or not a trial reflection condition. For a valid reflection condition, one expects the former value to be considerably larger than the latter. In Section 3.1 of Palatinus & van der Lee (2008), real examples of marginal cases are described.

[3] The tables in Appendix 1.4.4 mentioned above actually deal with space groups in reciprocal space; however, the left part of any entry is just the indices of a reflection generated by the point-group operation corresponding to this entry.

Table 1.6.2.1
The ability of the procedures described in Sections 1.6.2.1 and 1.6.5.1 to distinguish between space groups

The columns of the table show the number of sets of space groups that are indistinguishable by the chosen technique, according to the number of space groups in the set, *e.g.* for Laue-class discrimination, 85 space groups may be uniquely identified, whereas there are 8 sets containing 5 space groups indistinguishable by this technique. The tables in Section 1.6.4 contain 416 different settings of space groups generated from the 230 space-group types.

	No. of space groups in set that are indistinguishable by procedure used					
	1	2	3	4	5	6
No. of sets for Laue-class discrimination	85	78	43	0	8	1
No. of sets for point-group discrimination	390	13	0	0	0	0

The third stage continues by noting that the systematic absences are characteristic of the space group of the crystal, although some sets of space groups have identical reflection conditions. In Chapter 2.3 one finds all the reflection conditions listed individually for the 230 space groups. For practical use in space-group determination, tables have been set up that present a list of all those space groups that are characterized by a given set of reflection conditions. The tables for all the Bravais lattices and Laue groups are given in Section 1.6.4 of this chapter. So, once the reflection conditions have been determined, all compatible space groups can be identified from the tables. Table 1.6.2.1 shows that 85 space groups may be unequivocally determined by the procedures defined in this section based on the identification of the Laue group. For other sets of reflection conditions, there are a larger number of compatible space groups, attaining the value of 6 in one case. It is appropriate at this point to anticipate the results presented in Section 1.6.5.1, which exploit the resonant-scattering contribution to the diffracted intensities and under appropriate conditions allow not only the Laue group but also the point group of the crystal to be identified. If such is the case, the last line of Table 1.6.2.1 shows that almost all space groups can be unequivocally determined. In the remaining 13 pairs of space groups, constituting 26 space groups in all, there are the 11 enantiomorphic pairs of space groups [($P4_1$–$P4_3$), ($P4_122$–$P4_322$), ($P4_12_12$–$P4_32_12$), ($P3_1$–$P3_2$), ($P3_121$–$P3_221$), ($P3_112$–$P3_212$), ($P6_1$–$P6_5$), ($P6_2$–$P6_4$), ($P6_122$–$P6_522$), ($P6_222$–$P6_422$) and ($P4_132$–$P4_332$)] and the two exceptional pairs of $I222$ & $I2_12_12_1$ and $I23$ & $I2_13$, characterized by having the same symmetry elements in a different arrangement in space. These 13 pairs of space groups cannot be distinguished by the methods described in Sections 1.6.2 and 1.6.5.1, but may be distinguished when a reliable atomic structural model of the crystal has been obtained. On the other hand, all these 13 pairs of space groups can be distinguished by the methods described in Section 1.6.6 and in detail in Saitoh *et al.* (2001). It should be pointed out in connection with this third stage that a possible weakness of the analysis of systematic absences for crystals with small unit-cell dimensions is that there may be a small number of axial reflections capable of being systematically absent.

It goes without saying that the selected space groups must be compatible with the Bravais lattice determined in stage 1, with the Laue class determined in stage 2 and with the set of space-group absences determined in stage 3.

We thank L. Palatinus (2011) for having drawn our attention to the unexploited potential of the Patterson function for the determination of the space group of the crystal. The discovery of

this method is due to Buerger (1946) and later obtained only a one-sentence reference by Rogers (1950) and by Rossmann & Arnold (2001). The method is based on the observation that interatomic vectors between symmetry-related (other than by inversion in a point) atoms cause peaks to accumulate in the corresponding Harker sections and lines of the Patterson function. It is thus only necessary to find the location of those Harker sections and lines that have a high concentration of peaks to identify the corresponding symmetry operations of the space group. At the time of its discovery, it was not considered an economic method of space-group determination due to the labour involved in calculating the Patterson function. Subsequently it was completely neglected and there are no recent reports of its use. It is thus not possible to report on its strengths and weaknesses in practical modern-day applications.

1.6.2.2. Structure-factor statistics and crystal symmetry

Most structure-solving software packages contain a section dedicated to several probabilistic methods based on the Wilson (1949) paper on the probability distribution of structure-factor magnitudes. These statistics sometimes correctly indicate whether the intensity data set was collected from a centrosymmetric or noncentrosymmetric crystal. However, not infrequently these indications are erroneous. The reasons for this may be many, but outstandingly important are (i) the presence of a few very heavy atoms amongst a host of lighter ones, and (ii) a very small number of nearly equal atoms. Omission of weak reflections from the data set also contributes to failures of Wilson (1949) statistics. These erroneous indications are also rather strongly space-group dependent.

The well known probability density functions (hereafter p.d.f.'s) of the magnitude of the normalized structure factor E, also known as ideal p.d.f.'s, are

$$p(|E|) = \begin{cases} \sqrt{2/\pi}\exp\left(-|E|^2/2\right) & \text{for } P\overline{1} \\ 2|E|\exp(-|E|^2) & \text{for } P1 \end{cases}, \qquad (1.6.2.3)$$

where it is assumed that all the atoms are of the same chemical element. Let us see their graphical representations.

It is seen from Fig. 1.6.2.1 that the two p.d.f.'s are significantly different, but usually they are not presented as such by the software. What is usually shown are the cumulative distributions of $|E|^2$, the moments: $\langle|E|^n\rangle$ for $n = 1, 2, 3, 4, 5, 6$, and the averages of low powers of $|E^2 - 1|$ for ideal centric and acentric distributions, based on equation (1.6.2.3). Table 1.6.2.2 shows the numerical values of several low-order moments of $|E|$ and that of the lowest power of $|E^2 - 1|$. The higher the value of n the greater is the difference between their values for centric and acentric cases. However, it is most important to remember that the influence of measurement uncertainties also increases with n and therefore the higher the moment the less reliable it tends to be.

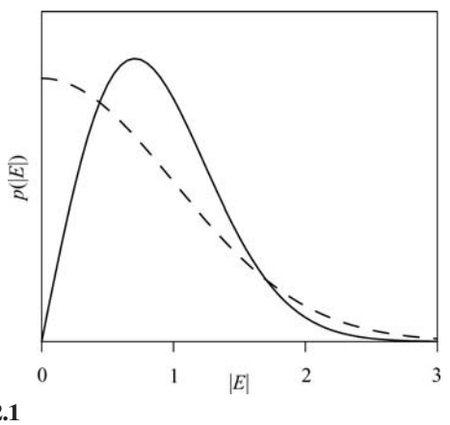

Figure 1.6.2.1
Ideal p.d.f.'s for the equal-atom case. The dashed line is the centric, and the solid line the acentric ideal p.d.f.

Table 1.6.2.2
The numerical values of several low-order moments of $|E|$, based on equation (1.6.2.3)

Moment	$P\overline{1}$	$P1$
$\langle\|E\|\rangle$	0.798	0.886
$\langle\|E\|^2\rangle$	1.000	1.000
$\langle\|E\|^3\rangle$	1.596	1.329
$\langle\|E\|^4\rangle$	3.000	2.000
$\langle\|E\|^5\rangle$	6.383	3.323
$\langle\|E\|^6\rangle$	15.000	6.000
$\langle\|E^2 - 1\|\rangle$	0.968	0.736

There are several ideal indicators of the status of centrosymmetry of a crystal structure. The most frequently used are: (i) the $N(z)$ test (Howells *et al.*, 1950), a cumulative distribution of $z = |E|^2$, based on equation (1.6.2.3), and (ii) the low-order moments of $|E|$, also based on equation (1.6.2.3). Equation (1.6.2.3), however, is very seldom used as an indicator of the status of centrosymmetry of a crystal stucture.

Let us now briefly consider p.d.f.'s that are valid for any atomic composition as well as any space-group symmetry, and exemplify their performance by comparing a histogram derived from observed intensities from a $P\overline{1}$ structure with theoretical p.d.f.'s for the space groups $P1$ and $P\overline{1}$. The p.d.f.'s considered presume that all the atoms are in general positions and that the reflections considered are general (see, *e.g.*, Section 1.6.3). A general treatment of the problem is given in the literature and summarized in the book *Introduction to Crystallographic Statistics* (Shmueli & Weiss, 1995).

The basics of the exact p.d.f.'s are conveniently illustrated in the following. The normalized structure factor for the space group $P\overline{1}$, assuming that all the atoms occupy general positions and resonant scattering is neglected, is given by

$$E(\mathbf{h}) = 2\sum_{j=1}^{N/2} n_j \cos(2\pi\mathbf{h}\boldsymbol{r}_j),$$

where n_j is the normalized scattering factor. The maximum possible value of E is $E_{\max} = \sum_{j=1}^{N} n_j$ and the minimum possible value of E is $-E_{\max}$. Therefore, $E(\mathbf{h})$ must be confined to the $(-E_{\max}, E_{\max})$ range. The probability of finding E outside this range is of course zero. Such a probability density function can be expanded in a Fourier series within this range (*cf.* Shmueli *et al.*, 1984). This is the basis of the derivation, the details of which are well documented (*e.g.* Shmueli *et al.*, 1984; Shmueli & Weiss, 1995; Shmueli, 2007). Exact p.d.f.'s for any centrosymmetric space group have the form

$$p(|E|) = \alpha\left\{1 + 2\sum_{m=1}^{\infty} C_m \cos(\pi m|E|\alpha)\right\}, \qquad (1.6.2.4)$$

where $\alpha = 1/E_{\max}$, and exact p.d.f.'s for any noncentrosymmetric space group can be computed as the double Fourier series

$$p(|E|) = \tfrac{1}{2}\pi\alpha^2|E|\sum_{m=1}^{\infty}\sum_{n=1}^{\infty} C_{mn} J_0[\pi\alpha|E|(m^2 + n^2)^{1/2}], \qquad (1.6.2.5)$$

where $J_0(X)$ is a Bessel function of the first kind and of order zero. Expressions for the coefficients C_m and C_{mn} are given by

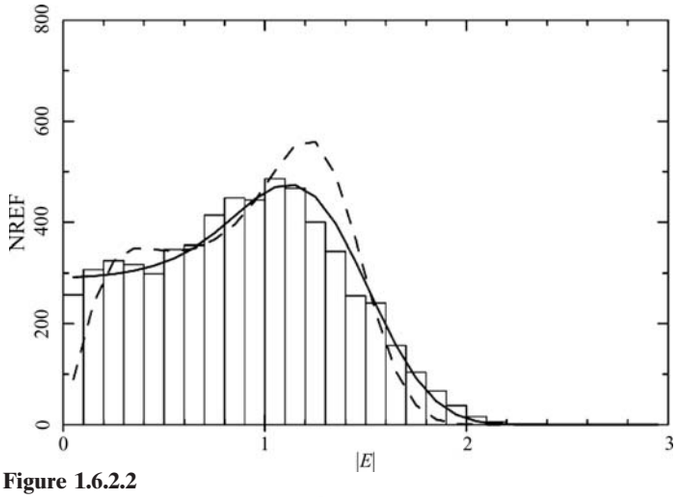

Figure 1.6.2.2
Exact p.d.f.'s. for a crystal of [(*Z*)-ethyl *N*-isopropylthiocarbamato-κS](tricyclohexylphosphine-κP)gold(I) in the triclinic system. Solid curve: $P\overline{1}$, computed from (1.6.2.4); dashed curve: *P*1, computed from (1.6.2.5); histogram based on the data computed from all the reflections with non-negative reduced intensities. The height of each bin corresponds to the number of reflections (NREF) in its range of $|E|$ values. The p.d.f.'s are scaled up to the histogram.

Rabinovich *et al.* (1991) and by Shmueli & Wilson (2008) for all the space groups up to and including $Fd\overline{3}$.

The following example deals with a very high sensitivity to atomic heterogeneity. Consider the crystal structure of [(*Z*)-ethyl *N*-isopropylthiocarbamato-κS](tricyclohexylphosphine-κP)gold(I), published as $P\overline{1}$ with $Z = 2$, the content of its asymmetric unit being $AuSPONC_{24}H_{45}$ (Tadbuppa & Tiekink, 2010). Let us construct a histogram from the $|E|$ data computed from all the observed reflections with non-negative reduced intensities and compare the histogram with the p.d.f.'s for the space groups *P*1 and $P\overline{1}$, computed from equations (1.6.2.5) and (1.6.2.4), respectively. The histogram and the p.d.f.'s were put on the same scale. The result is shown in Fig. 1.6.2.2.

A visual comparison strongly indicates that the space-group assignment as $P\overline{1}$ was correct, since the recalculated histogram agrees rather well with the p.d.f. (1.6.2.4) and much less with (1.6.2.5). The ideal Wilson-type statistics incorrectly indicated that this crystal is noncentrosymmetric. It is seen that the ideal p.d.f. breaks down in the presence of strong atomic heterogeneity (gold among many lighter atoms) in the space group $P\overline{1}$. Other space groups behave differently, as shown in the literature (*e.g.* Rabinovich *et al.*, 1991; Shmueli & Weiss, 1995).

Additional examples of applications of structure-factor statistics and some relevant computing considerations and software can be found in Shmueli (2012) and Shmueli (2013).

1.6.2.3. Symmetry information from the structure solution

It is also possible to obtain information on the symmetry of the crystal after structure solution. The latter is obtained either in space group *P*1 (*i.e.* no symmetry assumed) or in some other candidate space group. The analysis may take place either on the electron-density map, or on its interpretation in terms of atomic coordinates and atomic types (*i.e.* chemical elements). The analysis of the electron-density map has become increasingly popular with the advent of dual-space methods, first proposed in the charge-flipping algorithm by Oszlányi & Sütő (2004), which solve structures in *P*1 by default. The analysis of the atomic coordinates and atomic types obtained from least-squares refinement in a candidate space group is used extensively in structure validation. Symmetry operations present in the structure solution but not in the candidate space group are sought.

An exhaustive search for symmetry operations is undertaken. However, those to be investigated may be very efficently limited by making use of knowledge of the highest point-group symmetry of the lattice compatible with the known cell dimensions of the crystal. It is well established that the point-group symmetry of any lattice is one of the following seven centrosymmetric point groups: $\overline{1}$, 2/*m*, *mmm*, 4/*mmm*, $\overline{3}m$, 6/*mmm*, $m\overline{3}m$. This point group is known as the holohedry of the lattice. The relationship between the symmetry operations of the space group and its holohedry is rather simple. A rotation or screw axis of symmetry in the crystal has as its counterpart a corresponding rotation axis of symmetry of the lattice and a mirror or glide plane in the crystal has as its counterpart a corresponding mirror plane in the lattice. The holohedry may be equal to or higher than the point group of the crystal. Hence, at least the rotational part of any space-group operation should have its counterpart in the symmetry of the lattice. If and when this rotational part is found by a systematic comparison either of the electron density or of the positions of the independent atoms of the solved structure, the location and intrinsic parts of the translation parts of the space-group operation can be easily completed.

Palatinus and van der Lee (2008) describe their procedure in detail with useful examples. It uses the structure solution both in the form of an electron-density map and a set of phased structure factors obtained by Fourier transformation. No interpretation of the electron-density map in the form of atomic coordinates and chemical-element type is required. The algorithm of the procedure proceeds in the following steps:

(1) The lattice centring is determined by a search for strong peaks in the autocorrelation (self-convolution, Patterson) function of the electron density and the potential centring vectors are evaluated through a reciprocal-space *R* value.
(2) A complete list of possible symmetry operations compatible with the lattice is generated by searching for the invariance of the direct-space metric under potential symmetry operations.
(3) A figure of merit is then assigned to each symmetry operation evaluated from the convolution of the symmetry-transformed electron density with that of the structure solution. Those symmetry operations that have a good figure of merit are selected as belonging to the space group of the crystal structure.
(4) The space group is completed by group multiplication of the selected operations and then validated.
(5) The positions of the symmetry elements are shifted to those of a conventional setting for the space group.

Palatinus & van der Lee (2008) report a very high success rate in the use of this algorithm. It is also a powerful technique to apply in structure validation.

Le Page's (1987) pioneering software *MISSYM* for the detection of 'missed' symmetry operations uses refined atomic coordinates, unit-cell dimensions and space group assigned from the crystal-structure solution. The algorithm follows all the principles described above in this section. In *MISSYM*, the metric symmetry is established as described in the first stage of Section 1.6.2.1. The 'missed' symmetry operations are those that are present in the arrangement of the atoms but are not part of the space group used for the structure refinement. Indeed, this procedure has its main applications in structure validation. The algorithm used in Le Page's software is also implemented in *ADDSYM* (Spek, 2003). There are numerous reports of successful applications of this software in the literature.

1.6.2.4. Restrictions on space groups

The values of certain chemical and physical properties of a bulk compound, or its crystals, have implications for the assignment of the space group of a crystal structure. In the chemical domain, notably in proteins and small-molecule natural products, information concerning the enantiomeric purity of the bulk compound or of its individual crystals is most useful. Further, all physical properties of a crystal are limited by the point group of the crystal structure in ways that depend on the individual nature of the physical property.

It is very well established that the crystal structure of an enantiomerically pure compound will be chiral (see Flack, 2003). By an enantiomerically pure compound one means a compound whose molecules are all chiral and all these molecules possess the same chirality. The space group of a chiral crystal structure will only contain the following types of symmetry operation: translations, pure rotations and screw rotations. Inversion in a point, mirror reflection or rotoinversion do not occur in the space group of a chiral crystal structure. Taking all this together means that the crystal structure of an enantiomerically pure compound will show one of 65 space groups (known as the Sohncke space groups), all noncentrosymmetric, containing only translations, rotations and screw rotations. As a consequence, the point group of a chiral crystal structure is limited to the 11 point groups containing only pure rotations (*i.e.* 1, 2, 222, 4, 422, 3, 32, 6, 622, 23 and 432). Particular attention must be paid as to whether a measurement of enantiomeric purity of a compound applies to the bulk material or to the single crystal used for the diffraction experiment. Clearly, a compound whose bulk is enantiomerically pure will produce crystals which are enantiomerically pure. The converse is not necessarily true (*i.e.* enantiomerically pure crystals do not necessarily come from an enantiomerically pure bulk). For example, a bulk compound which is a racemate (*i.e.* an enantiomeric mixture containing 50% each of the opposite enantiomers) may produce either (*a*) crystals of the racemic compound (*i.e.* crystals containing 50% each of the opposite enantiomers) or (*b*) a racemic conglomerate (*i.e.* a mixture of enantiomerically pure crystals in a proportion of 50% of each pure enantiomer) or (*c*) some other rarer crystallization modes. Consequently, as part of a single-crystal structure analysis, it is highly recommended to make a measurement of the enantiomeric purity of the single crystal used for the diffraction experiment.

Much information on methods of establishing the enantiomeric purity of a compound can be found in a special issue of *Chirality* devoted to the determination of absolute configuration (Allenmark *et al.*, 2007). Measurements in the fluid state of optical activity, optical rotatory dispersion (ORD), circular dichroism (CD) and enantioselective chromatography are of prime importance. Many of these are sufficiently sensitive to be applicable not only to the bulk compound but also to the single crystal used for the diffraction experiment taken into solution. CD may also be applied in the solid state.

Many physical properties of a crystalline solid are anisotropic and the symmetry of a physical property of a crystal is limited both by the point-group symmetry of the crystal and by symmetries inherent to the physical property under study. For further information on this topic see Part 1 of Volume D (Authier *et al.*, 2014). Unfortunately, many of these physical properties are intrinsically centrosymmetric, so few of them are of use in distinguishing between the subgroups of a Laue group, a common problem in space-group determination. In Chapter 3.2 of the present volume, Hahn & Klapper show to which point groups a crystal must belong to be capable of displaying some of the principal physical properties of crystals (Table 3.2.2.1). Measurement of morphology, pyroelectricity, piezoelectricity, second harmonic generation and optical activity of a crystalline sample can be of use.

1.6.2.5. Pitfalls in space-group determination

The methods described in Sections 1.6.2 and 1.6.5.1 rely on the crystal measured being a single-domain crystal, *i.e.* it should not be twinned. Nevertheless, some types of twin are easily identified at the measurement stage as they give rise to split reflections. Powerful data-reduction techniques may be applied to data from such crystals to produce a reasonably complete single-domain intensity data set. Consequently, the multi-domain twinned crystals that give rise to difficulties in space-group determination are those for which the reciprocal lattices of the individual domains overlap exactly without generating any splitting of the Bragg reflections. A study of the intensity data from such a crystal may display two anomalies. Firstly, the intensity distribution, as described and analysed in Section 1.6.2.2, will be broader than that of the monodomain crystal. Secondly, one may obtain a set of conditions for reflections that does not correspond to any entry in Section 1.6.4. In this chapter we give no further information on the determination of the space group for such twinned crystals. For further information on this topic see Part 3 of Volume D (Boček *et al.*, 2006) and Chapter 1.3 on twinning in Volume C (Koch, 2006). A supplement (Flack, 2015) to the current section deals with the determination of the space group from twinned crystals and those displaying a specialized metric. However, it is apposite to note that the existence of twins with overlapping reciprocal lattices can be identified by recording atomic resolution transmission electron-microscope images.

In order to obtain reliable results from space-group determination, the coverage of the reciprocal space by the intensity measurements should be as complete as possible. One should attempt to attain full-sphere data coverage, *i.e.* a complete set of intensity measurements in the point group 1. All Friedel opposites should be measured. The validity and reliability of the intensity statistics described in Section 1.6.2.2 rest on a full coverage of reciprocal lattice. Any systematic omission by resolution, azimuth and declination, intensity *etc.* of part of the asymmetric region of the reciprocal lattice has an adverse effect. In particular, reflections of weak intensity should not be omitted or deleted.

There are a few other common difficulties in space-group determination due either to the nature of the crystal or the experimental setup:

(*a*) The crystal may display a pseudo-periodicity leading to systematic series of weak or very weak reflections that can be mistaken for systematic absences.

(*b*) The physical effect of multiple reflections can lead to diffraction intensity appearing at the place of systematic absences. However, the shape of these multiple-reflection intensities is usually much sharper than a normal Bragg reflection.

(*c*) Contamination of the incident radiation by a $\lambda/2$ component may also cause intensity due to the $2h\,2k\,2l$ reflection to appear at the place of the hkl one. Kirschbaum *et al.* (1997) and Macchi *et al.* (1998) have studied this probem and describe ways of circumventing it.

1.6.3. Theoretical background of reflection conditions

By U. Shmueli

We shall now examine the effect of the space-group symmetry on the structure-factor function. These effects are of importance in the determination of crystal symmetry. If $(\boldsymbol{W}, \boldsymbol{w})$ is the matrix–column pair of a representative symmetry operation of the space group of the crystal, then, by definition

$$\rho(\boldsymbol{x}) = \rho(\boldsymbol{W}\boldsymbol{x} + \boldsymbol{w}), \tag{1.6.3.1}$$

where $\rho(\boldsymbol{x})$ is the value of the electron-density function at the point with coordinates $\boldsymbol{x}$, $\boldsymbol{W}$ is a matrix of proper or improper rotation and $\boldsymbol{w}$ is a translation part (*cf.* Section 1.2.2.1). It is known that the electron-density function at the point $\boldsymbol{x}$ is given by

$$\rho(\boldsymbol{x}) = \frac{1}{V}\sum_{\mathbf{h}} F(\mathbf{h}) \exp(-2\pi i \mathbf{h}\boldsymbol{x}), \tag{1.6.3.2}$$

where, in this and the following equations, $\mathbf{h}$ is the row matrix $(h\,k\,l)$ and $\boldsymbol{x}$ is a column matrix containing x, y and z in the first, second and third rows, respectively. Of course, $\mathbf{h}\boldsymbol{x}$ is simply equivalent to $hx + ky + lz$. If we substitute (1.6.3.2), with $\boldsymbol{x}$ replaced by $(\boldsymbol{W}\boldsymbol{x} + \boldsymbol{w})$ in (1.6.3.1) we obtain, after some calculation,

$$F(\mathbf{h}\boldsymbol{W}) = F(\mathbf{h}) \exp(-2\pi i \mathbf{h}\boldsymbol{w}). \tag{1.6.3.3}$$

Equation (1.6.3.3) is the fundamental relation between symmetry-related reflections (*e.g.* Waser, 1955; Wells, 1965; and Chapter 1.4 in Volume B). If we write $F(\mathbf{h}) = |F(\mathbf{h})| \exp[i\varphi(\mathbf{h})]$, equation (1.6.3.3) leads to the following relationships:

$$|F(\mathbf{h}\boldsymbol{W})| = |F(\mathbf{h})| \tag{1.6.3.4}$$

and

$$\varphi(\mathbf{h}\boldsymbol{W}) = \varphi(\mathbf{h}) - 2\pi\mathbf{h}\boldsymbol{w}. \tag{1.6.3.5}$$

Equation (1.6.3.4) indicates the equality of the intensities of truly symmetry-related reflections, while equation (1.6.3.5) relates the phases of the corresponding structure factors. The latter equation is of major importance in direct methods of phase determination [*e.g.* Chapter 2.2 in Volume B (Giacovazzo, 2008)].

We can now approach the problem of systematically absent reflections, which are alternatively called the conditions for possible reflections.

The reflection $\mathbf{h}$ is *general* if its indices remain unchanged *only* under the identity operation of the point group of the diffraction pattern. *I.e.*, if $\boldsymbol{W}$ is the matrix of the identity operation of the point group, the relation $\mathbf{h}\boldsymbol{W} = \mathbf{h}$ holds true. So, if the reflection $\mathbf{h}$ is general, we must have $\boldsymbol{W} \equiv \boldsymbol{I}$, where $\boldsymbol{I}$ is the identity matrix and, obviously, $\mathbf{h}\boldsymbol{I} = \mathbf{h}$. The operation $(\boldsymbol{I}, \boldsymbol{w})$ can be a space-group symmetry operation only if $\boldsymbol{w}$ is a lattice vector. Let us denote it by $\boldsymbol{w}_L$. Equation (1.6.3.3) then reduces to

$$F(\mathbf{h}) = F(\mathbf{h}) \exp(-2\pi i \mathbf{h}\boldsymbol{w}_L) \tag{1.6.3.6}$$

and $F(\mathbf{h})$ can be nonzero only if $\exp(-2\pi i \mathbf{h}\boldsymbol{w}_L) = 1$. This, in turn, is possible only if $\mathbf{h}\boldsymbol{w}_L$ is an integer and leads to conditions depending on the lattice type. For example, if the components of $\boldsymbol{w}_L$ are all integers, which is the case for a *P*-type lattice, the above condition is fulfilled for all $\mathbf{h}$ – the lattice type does not impose any restrictions. If the lattice is of type *I*, there are two lattice points in the unit cell, at say 0, 0, 0 and 1/2, 1/2, 1/2. The first of these does not lead to any restrictions on possible reflections. The second, however, requires that $\exp[-\pi i(h + k + l)]$ be equal to unity. Since $\exp(\pi i n) = (-1)^n$, where n is an integer, the possible reflections from a crystal with an *I*-type lattice must have indices such that their sum is an even integer; if the sum of the indices is an odd integer, the reflection is *systematically absent*. In this way, we examine all lattice types for conditions of possible reflections (or systematic absences) and present the results in Table 1.6.3.1.

The reflection $\mathbf{h}$ is *special* if it remains unchanged under at least one operation of the point group of the diffraction pattern in addition to its identity operation. *I.e.*, the relation $\mathbf{h}\boldsymbol{W} = \mathbf{h}$ holds true for more than one operation of the point group. We shall now assume that the reflection $\mathbf{h}$ is special. By definition, this reflection remains invariant under more than one operation of the point group of the diffraction pattern. These operations form a subgroup of the point group of the diffraction pattern, known as the stabilizer (formerly called the *isotropy subgroup*) of the reflection $\mathbf{h}$, and we denote it by the symbol $\mathcal{S}_{\mathbf{h}}$. For each space-group symmetry operation $(\boldsymbol{W}, \boldsymbol{w})$ where $\boldsymbol{W}$ is the matrix of an element of $\mathcal{S}_{\mathbf{h}}$ we must therefore have $\mathbf{h}\boldsymbol{W} = \mathbf{h}$. Equation (1.6.3.3) now reduces to

$$F(\mathbf{h}) = F(\mathbf{h}) \exp(-2\pi i \mathbf{h}\boldsymbol{w}). \tag{1.6.3.7}$$

Of course, if $\boldsymbol{W}$ represents the identity operation, $\boldsymbol{w}$ must be a lattice vector and the discussion summarized in Table 1.6.3.1 applies. We therefore require that $\boldsymbol{W}$ is the matrix of an element of $\mathcal{S}_{\mathbf{h}}$ other than the identity. $F(\mathbf{h})$ can be nonzero only if the exponential factor in (1.6.3.7) equals unity. This, in turn, is possible only if $\mathbf{h}\boldsymbol{w}$ is an integer.

Let us consider a monoclinic crystal with *P*-type lattice (*i.e.* with an *mP*-type Bravais lattice) and a *c*-glide reflection as an example. Assuming $\mathbf{b}$ perpendicular to the $\mathbf{ac}$ plane, the $(\boldsymbol{W}, \boldsymbol{w})$ representation of *c* is given by

$$c\colon \left[\begin{pmatrix} 1 & 0 & 0 \\ 0 & \overline{1} & 0 \\ 0 & 0 & 1 \end{pmatrix}, \begin{pmatrix} 0 \\ y \\ 1/2 \end{pmatrix}\right].$$

The indices of reflections that remain unchanged under the application of the mirror component of the glide-reflection operation must be $h0l$. The translation part of the *c*-glide-reflection operation has the form $(0, y, 1/2)$, where $y = 0$ corresponds to the plane passing through the origin. Hence, for any value of y, the scalar product $\mathbf{h}\boldsymbol{w}$ is $l/2$ and the necessary condition for a nonzero value of an $h0l$ reflection is $l = 2n$, where n is an integer. Intensities of $h0l$ reflections with odd l will be *systematically absent*.

Table 1.6.3.2 shows the effect of some glide reflections on reflection conditions.[4]

Let us now assume a crystal with an *mP*-type Bravais lattice and a twofold screw axis taken as being parallel to $\mathbf{b}$. The $(\boldsymbol{W}, \boldsymbol{w})$ representation of the corresponding screw rotation is given by

$$2_1\colon \left[\begin{pmatrix} \overline{1} & 0 & 0 \\ 0 & 1 & 0 \\ 0 & 0 & \overline{1} \end{pmatrix}, \begin{pmatrix} x \\ 1/2 \\ z \end{pmatrix}\right].$$

The diffraction indices that remain unchanged upon the application of the rotation part of 2_1 must be of the form $(0k0)$. The translation part of the screw operation is of the form $(x, 1/2, z)$, where the values of x and z depend on the location of the origin. Hence, for any values of x and z the scalar product $\mathbf{h}\boldsymbol{w}$ is $k/2$ and the necessary condition for a nonzero value of a $0k0$ reflection is

[4] The reflection condition in the fourth line of Table 1.6.3.2 is a consequence of the fact that a *d* glide appears only with Bravais lattices of types *I* and *F*.

Table 1.6.3.1
Effect of lattice type on conditions for possible reflections

Lattice type	$\boldsymbol{w}_L^T$	$\mathbf{h}\boldsymbol{w}_L$	Conditions for possible reflections
P	(0, 0, 0)	Integer	None
A	$(0, \frac{1}{2}, \frac{1}{2})$	$(k+l)/2$	hkl: $k+l=2n$
B	$(\frac{1}{2}, 0, \frac{1}{2})$	$(h+l)/2$	hkl: $h+l=2n$
C	$(\frac{1}{2}, \frac{1}{2}, 0)$	$(h+k)/2$	hkl: $h+k=2n$
I	$(\frac{1}{2}, \frac{1}{2}, \frac{1}{2})$	$(h+k+l)/2$	hkl: $h+k+l=2n$
F	$(0, \frac{1}{2}, \frac{1}{2})$	$(k+l)/2$	h, k and l are all even or all odd (simultaneous fulfillment of the conditions for types A, B and C).
	$(\frac{1}{2}, 0, \frac{1}{2})$	$(h+l)/2$	
	$(\frac{1}{2}, \frac{1}{2}, 0)$	$(h+k)/2$	
$R_{\rm obv}$	$(\frac{2}{3}, \frac{1}{3}, \frac{1}{3})$	$(2h+k+l)/3$	hkl: $-h+k+l=3n$
	$(\frac{1}{3}, \frac{2}{3}, \frac{2}{3})$	$(h+2k+2l)/3$	(triple hexagonal cell in obverse orientation)
$R_{\rm rev}$	$(\frac{1}{3}, \frac{2}{3}, \frac{1}{3})$	$(h+2k+l)/3$	hkl: $h-k+l=3n$
	$(\frac{2}{3}, \frac{1}{3}, \frac{2}{3})$	$(2h+k+2l)/3$	(triple hexagonal cell in reverse orientation)

Table 1.6.3.2
Effect of some glide reflections on conditions for possible reflections

Glide reflection	$\boldsymbol{w}^T$	$\mathbf{h}$	Conditions for possible reflections
$a \perp [001]$	(1/2, 0, z)	(hk0)	hk0: $h=2n$
$b \perp [001]$	(0, 1/2, z)	(hk0)	hk0: $k=2n$
$n \perp [001]$	(1/2, 1/2, z)	(hk0)	hk0: $h+k=2n$
$d \perp [001]$	(1/4, $\pm$1/4, z)	(hk0)	hk0: $h+k=4n$ (h, $k=2n$)

Table 1.6.3.3
Effect of some screw rotations on conditions for possible reflections

Screw rotation	$\boldsymbol{w}^T$	$\mathbf{h}$	Conditions for possible reflections
$2_1 \parallel [100]$	(1/2, y, z)	(h00)	h00: $h=2n$
$2_1 \parallel [010]$	(x, 1/2, z)	(0k0)	0k0: $k=2n$
$2_1 \parallel [001]$	(x, y, 1/2)	(00l)	00l: $l=2n$
$2_1 \parallel [110]$	(1/2, 1/2, z)	(hh0)	None
$3_1 \parallel [001]$	(x, y, 1/3)	(00l)	00l: $l=3n$
$3_1 \parallel [111]$	(1/3, 1/3, 1/3)	(hhh)	None
$4_1 \parallel [001]$	(x, y, 1/4)	(00l)	00l: $l=4n$
$6_1 \parallel [001]$	(x, y, 1/6)	(00l)	00l: $l=6n$

$k=2n$. 0k0 reflections with odd k will be systematically absent. A brief summary of the effects of various screw rotations on the conditions for possible reflections from the corresponding special subsets of hkl is given in Table 1.6.3.3. Note, however, that while the presence of a twofold screw axis parallel to **b** ensures the condition 0k0: $k=2n$, the actual observation of such a condition can be taken as an indication but not as absolute proof of the presence of a screw axis in the crystal.

It is interesting to note that some diagonal screw axes do not give rise to conditions for possible reflections. For example, let $\boldsymbol{W}$ be the matrix of a threefold rotation operation parallel to [111] and $\boldsymbol{w}^T$ be given by (1/3, 1/3, 1/3). It is easy to show that the diffraction vector that remains unchanged when postmultiplied by $\boldsymbol{W}$ has the form $\mathbf{h}=(hhh)$ and, obviously, for such **h** and $\boldsymbol{w}$, $\mathbf{h}\boldsymbol{w}=h$. Since this scalar product is an integer there are, according to equation (1.6.3.7), no values of the index h for which the structure factor $F(hhh)$ must be absent.

A short discussion of special reflection conditions

The conditions for possible reflections arising from lattice types, glide reflections and screw rotations are related to general equivalent positions and are known as *general reflection conditions*. There are also *special* or '*extra*' reflection conditions that arise from the presence of atoms in special positions. These conditions are observable if the atoms located in special positions are much heavier than the rest. The minimal special conditions are listed in the space-group tables in Chapter 2.3. They can sometimes be understood if the geometry of a given specific site is examined. For example, Wyckoff position 4i in space group $P4_222$ (93) can host four atoms, at coordinates

$$4i\colon\ 0, \tfrac{1}{2}, z;\ \ \tfrac{1}{2}, 0, z+\tfrac{1}{2};\ \ 0, \tfrac{1}{2}, \overline{z};\ \ \tfrac{1}{2}, 0, \overline{z}+\tfrac{1}{2}.$$

It is seen that the second and fourth coordinates are obtained from the first and third coordinates, respectively, upon the addition of the vector $t(\frac{1}{2}, \frac{1}{2}, \frac{1}{2})$. An additional I-centring is therefore present in this set of special positions. Hence, the special reflection condition for this set is hkl: $h+k+l=2n$.

It should be pointed out, however, that only the general reflection conditions are used for a complete or partial determination of the space group and that the special reflection conditions only apply to spherical atoms. By the latter assumption we understand not only the assumption of spherical distribution of the atomic electron density but also isotropic displacement parameters of the equivalent atoms that belong to the set of corresponding special positions.

One method of finding the minimal special reflection conditions for a given set of special positions is the evaluation of the trigonometric structure factor for the set in question. For example, consider the Wyckoff position 4c of the space group $Pbcm$ (57). The coordinates of the special equivalent positions are

$$4c\colon\ \ x, \tfrac{1}{4}, 0;\quad \overline{x}, \tfrac{3}{4}, \tfrac{1}{2};\quad \overline{x}, \tfrac{3}{4}, 0;\quad x, \tfrac{1}{4}, \tfrac{1}{2}$$

and the corresponding trigonometric structure factor is

$$S(\mathbf{h}) = \exp\left[2\pi i\left(hx+\frac{k}{4}\right)\right] + \exp\left[2\pi i\left(-hx+\frac{3k}{4}+\frac{l}{2}\right)\right] + \exp\left[2\pi i\left(-hx+\frac{3k}{4}\right)\right] + \exp\left[2\pi i\left(hx+\frac{k}{4}+\frac{l}{2}\right)\right].$$

It can be easily shown that

$$S(\mathbf{h}) = 2\cos\left[2\pi\left(hx+\frac{k}{4}\right)\right][1+\exp(\pi i l)]$$

and the last factor equals 2 for l even and equals zero for l odd. The special reflection condition is therefore: hkl: $l=2n$.

Another approach is provided by considerations of the eigensymmetry group and the extraordinary orbits of the space group (see Section 1.4.4.4). We recall that the eigensymmetry group is a group of all the operations that leave the orbit of a point under the space group considered invariant, and the extraordinary orbit is associated with the eigensymmetry group that contains translations not present in the space group (see Chapter 1.4). In the above example the orbit is extraordinary, since its eigensymmetry group contains a translation corresponding to $\frac{1}{2}\mathbf{c}$. If this is taken as a basis vector, we have the Laue equation $\frac{1}{2}\mathbf{c}\cdot\mathbf{h}=l'$, where **h** is represented as a reciprocal-lattice vector and l' is an integer which also equals $l/2$. But for $l/2$ to be an integer we must have even l. We again obtain the condition hkl: $l=2n$.

These reflection conditions that are not related to space-group operations are given in Chapter 2.3 only for special positions. They may arise, however, also for different reasons. For example, a heavy atom at the origin of the space group $P2_12_12_1$ would generate *F*-centring with corresponding apparent absences (*cf.* the special position 4*a* of the space group *Pbca* and the absences it generates).

We wish to point out that the most common 'special-position absence' in molecular structures is due to a heavy atom at the origin of the space group $P2_1/c$.

1.6.4. Tables of reflection conditions and possible space groups

By H. D. Flack and U. Shmueli

1.6.4.1. Introduction

The primary order of presentation of these tables of reflection conditions of space groups is the Bravais lattice. This order has been chosen because cell reduction on unit-cell dimensions leads to the Bravais lattice as described as stage 1 in Section 1.6.2.1. Within the space groups of a given Bravais lattice, the entries are arranged by Laue class, which may be obtained as described as stage 2 in Section 1.6.2.1. As a consequence of these decisions about the way the tables are structured, in the hexagonal family one finds for the Bravais lattice *hP* that the Laue classes $\overline{3}$, $\overline{3}m1$, $\overline{3}1m$, 6/*m* and 6/*mmm* are grouped together.

As an aid in the study of naturally occurring macromolecules and compounds made by enantioselective synthesis, the space groups of enantiomerically pure compounds (Sohncke space groups) are typeset in bold.

The tables show, on the left, sets of reflection conditions and, on the right, those space groups that are compatible with the given set of reflection conditions. The reflection conditions, *e.g.* *h* or $k + l$, are to be understood as $h = 2n$ or $k + l = 2n$, respectively. All of the space groups in each table correspond to the same Patterson symmetry, which is indicated in the table header. This makes for easy comparison with the entries for the individual space groups in Chapter 2.3 of this volume, in which the Patterson symmetry is also very clearly shown. All space groups with a conventional choice of unit cell are included in Tables 1.6.4.2–1.6.4.30. All alternative settings displayed in Chapter 2.3 are thus included. The following further alternative settings, not displayed in Chapter 2.3, are also included: space group $Pb\overline{3}$ (205) and all the space groups with an *hR* Bravais lattice in the reverse setting with hexagonal axes.

Table 1.6.2.1 gives some relevant statistics drawn from Tables 1.6.4.2–1.6.4.30. The total number of space-group settings mentioned in these tables is 416. This number is considerably larger than the 230 space-group types described in Part 2 of this volume. The following example shows why the tables include data for several descriptions of the space-group types. At the stage of space-group determination for a crystal in the crystal class *mm*2, it is not yet known whether the twofold rotation axis lies along **a**, **b** or **c**. Consequently, space groups based on the three point groups 2*mm,* *m*2*m* and *mm*2 need to be considered.

In some texts dealing with space-group determination, a 'diffraction symbol' (sometimes also called an 'extinction symbol') in the form of a Hermann–Mauguin space-group symbol is used as a shorthand code for the reflection conditions and Laue class. These symbols were introduced by Buerger (1935, 1942, 1969) and a concise description is to be found in Looijenga-Vos & Buerger (2002). Nespolo *et al.* (2014) use them.

1.6.4.2. Examples of the use of the tables

(1) If the Bravais lattice is *oI* and the Laue class is *mmm*, Table 1.6.4.1 directs us to Table 1.6.4.11. Given the observed reflection conditions

$$hkl\colon h + k + l = 2n, \quad 0kl\colon k = 2n, l = 2n, \quad h0l\colon h + l = 2n,$$
$$hk0\colon h + k = 2n, \quad h00\colon h = 2n, \quad 0k0\colon k = 2n, \quad 00l\colon l = 2n,$$

it is seen from Table 1.6.4.11 that the possible settings of the space groups are: *Ibm*2 (46), *Ic*2*m* (46), *Ibmm* (74) and *Icmm* (74).

(2) If the Bravais lattice is *oP* and the Laue class is *mmm*, Table 1.6.4.1 directs us to Table 1.6.4.7. If there are no conditions on 0*kl*, the space groups *P*222 to *Pmnn* should be searched. If the condition is 0*kl*: $k = 2n$ or $l = 2n$, the space groups *Pbm*2 to *Pcnn* should be searched. If the condition is 0*kl*: $k + l = 2n$, the space groups $Pnm2_1$ to *Pnnn* should be searched.

(3) If the Bravais lattice is *cP* and the Laue class is $m\overline{3}$, Table 1.6.4.1 directs us to Table 1.6.4.25. If the conditions are 0*kl*: $k = 2n$ and *h*00: $h = 2n$, it is readily seen that the space group is $Pa\overline{3}$.

(4) If only the Bravais lattice is known or assumed, which is the case in powder-diffraction work (see Section 1.6.5.3), all tables of this section corresponding to this Bravais lattice need to be consulted. For example, if it is known that the Bravais lattice is of type *cP*, Table 1.6.4.1 tells us that the possible Laue classes are $m\overline{3}$ and $m\overline{3}m$, and the possible space groups can be found in Tables 1.6.4.25 and 1.6.4.26, respectively. The appropriate reflection conditions are of course given in these tables. All relevant tables can thus be located with the aid of Table 1.6.4.1 if the Bravais lattice is known.

1.6.5. Specialized methods of space-group determination

By H. D. Flack

1.6.5.1. Applications of resonant scattering to symmetry determination

1.6.5.1.1. Introduction

In small-molecule crystallography, it has been customary in crystal-structure analysis to make no use of the contribution of resonant scattering (otherwise called anomalous scattering and in older literature anomalous dispersion) other than in the specific area of absolute-structure and absolute-configuration determination. One may trace the causes of this situation to the weakness of the resonant-scattering contribution, to the high cost in time and labour of collecting intensity data sets containing measurements of all Friedel opposites and for a lack of any perceived or real need for the additional information that might be obtained from the effects of resonant scattering.

On the experimental side, the turning point came with the widespread distribution of area detectors for small-molecule crystallography, giving the potential to measure, at no extra cost, full-sphere data sets leading to the intensity differences between Friedel opposites *hkl* and $\overline{hkl}$. In 2015, the new methods of data analysis briefly presented here are in the stage of development

(*continued on page* 125)

Table 1.6.4.1
Summary of Tables 1.6.4.2–1.6.4.30

Table No.	Bravais lattice	Laue class	Patterson symmetry	Comment
1.6.4.2	*aP*	$\bar{1}$	$P\bar{1}$	
1.6.4.3	*mP*	2/*m*	*P*12/*m*1	Unique *b*
1.6.4.4	*mS* (*mC*, *mA*, *mI*)	2/*m*	*C*12/*m*1, *A*12/*m*1, *I*12/*m*1	Unique *b*
1.6.4.5	*mP*	2/*m*	*P*112/*m*	Unique *c*
1.6.4.6	*mS* (*mA*, *mB*, *mI*)	2/*m*	*A*112/*m*, *B*112/*m*, *I*112/*m*	Unique *c*
1.6.4.7	*oP*	*mmm*	*Pmmm*	
1.6.4.8	*oS* (*oC*)	*mmm*	*Cmmm*	
1.6.4.9	*oS* (*oB*)	*mmm*	*Bmmm*	
1.6.4.10	*oS* (*oA*)	*mmm*	*Ammm*	
1.6.4.11	*oI*	*mmm*	*Immm*	
1.6.4.12	*oF*	*mmm*	*Fmmm*	
1.6.4.13	*tP*	4/*m*	*P*4/*m*	
1.6.4.14	*tP*	4/*mmm*	*P*4/*mmm*	
1.6.4.15	*tI*	4/*m*	*I*4/*m*	
1.6.4.16	*tI*	4/*mmm*	*I*4/*mmm*	
1.6.4.17	*hP*	$\bar{3}$	$P\bar{3}$	
1.6.4.18	*hP*	$\bar{3}1m$ and $\bar{3}m1$	$P\bar{3}1m$ and $P\bar{3}m1$	
1.6.4.19	*hP*	6/*m*	*P*6/*m*	
1.6.4.20	*hP*	6/*mmm*	*P*6/*mmm*	
1.6.4.21	*hR*	$\bar{3}$	$R\bar{3}$	Hexagonal axes
1.6.4.22	*hR*	$\bar{3}m$	$R\bar{3}m$	Hexagonal axes
1.6.4.23	*hR*	$\bar{3}$	$R\bar{3}$	Rhombohedral axes
1.6.4.24	*hR*	$\bar{3}m$	$R\bar{3}m$	Rhombohedral axes
1.6.4.25	*cP*	$m\bar{3}$	$Pm\bar{3}$	
1.6.4.26	*cP*	$m\bar{3}m$	$Pm\bar{3}m$	
1.6.4.27	*cI*	$m\bar{3}$	$Im\bar{3}$	
1.6.4.28	*cI*	$m\bar{3}m$	$Im\bar{3}m$	
1.6.4.29	*cF*	$m\bar{3}$	$Fm\bar{3}$	
1.6.4.30	*cF*	$m\bar{3}m$	$Fm\bar{3}m$	

Table 1.6.4.2
Reflection conditions and possible space groups with Bravais lattice *aP* and Laue class $\bar{1}$; Patterson symmetry $P\bar{1}$

Reflection conditions	Space group	No.	Space group	No.
	***P*1**	1	$P\bar{1}$	2

Table 1.6.4.3
Reflection conditions and possible space groups with Bravais lattice *mP* and Laue class 2/*m*; (monoclinic, unique axis *b*); Patterson symmetry *P*12/*m*1

Reflection conditions						Space group	No.	Space group	No.	Space group	No.
*h*0*l*	0*kl*	*hk*0	0*k*0	*h*00	00*l*						
						***P*2**	3	*Pm*	6	*P*2/*m*	10
			k			***P*2$_1$**	4	*P*2$_1$/*m*	11		
h				*h*		*Pa*	7	*P*2/*a*	13		
h			*k*	*h*		*P*2$_1$/*a*	14				
l					*l*	*Pc*	7	*P*2/*c*	13		
l			*k*		*l*	*P*2$_1$/*c*	14				
h + *l*				*h*	*l*	*Pn*	7	*P*2/*n*	13		
h + *l*			*k*	*h*	*l*	*P*2$_1$/*n*	14				

Table 1.6.4.4
Reflection conditions and possible space groups with Bravais lattice *mS* (*mC*, *mA*, *mI*) and Laue class 2/*m* (monoclinic, unique axis *b*); Patterson symmetry *C*12/*m*1, *A*12/*m*1, *I*12/*m*1

Reflection conditions							Space group	No.	Space group	No.	Space group	No.
hkl	*h*0*l*	0*kl*	*hk*0	0*k*0	*h*00	00*l*						
$h + k$	h	k	$h + k$	k	h		***C*2**	5	*Cm*	8	*C*2/*m*	12
$h + k$	h, l	k	$h + k$	k	h	l	*Cc*	9	*C*2/*c*	15		
$k + l$	l	$k + l$	k	k		l	***A*2**	5	*Am*	8	*A*2/*m*	12
$k + l$	h, l	$k + l$	k	k	h	l	*An*	9	*A*2/*n*	15		
$h + k + l$	$h + l$	$k + l$	$h + k$	k	h	l	***I*2**	5	*Im*	8	*I*2/*m*	12
$h + k + l$	h, l	$k + l$	$h + k$	k	h	l	*Ia*	9	*I*2/*a*	15		

Table 1.6.4.5
Reflection conditions and possible space groups with Bravais lattice *mP* and Laue class 2/*m* (monoclinic, unique axis *c*); Patterson symmetry *P*112/*m*

Reflection conditions						Space group	No.	Space group	No.	Space group	No.
*h*0*l*	0*kl*	*hk*0	0*k*0	*h*00	00*l*						
						***P*2**	3	*Pm*	6	*P*2/*m*	10
					l	***P*2$_1$**	4	*P*2$_1$/*m*	11		
		h		h		*Pa*	7	*P*2/*a*	13		
		h		h	l	*P*2$_1$/*a*	14				
		k	k			*Pb*	7	*P*2/*b*	13		
		k	k		l	*P*2$_1$/*b*	14				
		$h + k$	k	h		*Pn*	7	*P*2/*n*	13		
		$h + k$	k	h	l	*P*2$_1$/*n*	14				

Table 1.6.4.6
Reflection conditions and possible space groups with Bravais lattice *mS* (*mA*, *mB*, *mI*) and Laue class 2/*m* (monoclinic, unique axis *c*); Patterson symmetry *A*112/*m*, *B*112/*m*1, *I*112/*m*

Reflection conditions							Space group	No.	Space group	No.	Space group	No.
hkl	*h*0*l*	0*kl*	*hk*0	0*k*0	*h*00	00*l*						
$k + l$	l	$k + l$	k	k		l	***A*2**	5	*Am*	8	*A*2/*m*	12
$k + l$	l	$k + l$	h, k	k	h	l	*Aa*	9	*A*2/*a*	15		
$h + l$	$h + l$	l	h		h	l	***B*2**	5	*Bm*	8	*B*2/*m*	12
$h + l$	$h + l$	l	h, k	k	h	l	*Bn*	9	*B*2/*n*	15		
$h + k + l$	$h + l$	$k + l$	$h + k$	k	h	l	***I*2**	5	*Im*	8	*I*2/*m*	12
$h + k + l$	$h + l$	$k + l$	h, k	k	h	l	*Ib*	9	*I*2/*b*	15		

Table 1.6.4.7
Reflection conditions and possible space groups with Bravais lattice *oP* and Laue class *mmm*; Patterson symmetry *Pmmm*

Reflection conditions						Space group	No.	Space group	No.	Space group	No.
0*kl*	*h*0*l*	*hk*0	*h*00	0*k*0	00*l*						
						***P*222** *P*2*mm*	16 25	*Pmm*2 *Pmmm*	25 47	*Pm*2*m*	25
					l	***P*222$_1$**	17				
				k		***P*22$_1$2**	17				
				k	*l*	***P*22$_1$2$_1$**	18				
			h			***P*2$_1$22**	17				
			h		*l*	***P*2$_1$22$_1$**	18				
			h	*k*		***P*2$_1$2$_1$2**	18				
			h	*k*	*l*	***P*2$_1$2$_1$2$_1$**	19				
		h	*h*			*P*2$_1$*ma*	26	*Pm*2*a*	28	*Pmma*	51
		k		*k*		*Pm*2$_1$*b*	26	*P*2*mb*	28	*Pmmb*	51
		h + *k*	*h*	*k*		*Pm*2$_1$*n*	31	*P*2$_1$*mn*	31	*Pmmn*	59
	h		*h*			*P*2$_1$*am*	26	*Pma*2	28	*Pmam*	51
	h	*h*	*h*			*P*2*aa*	27	*Pmaa*	49		
	h	*k*	*h*	*k*		*P*2$_1$*ab*	29	*Pmab*	57		
	h	*h* + *k*	*h*	*k*		*P*2*an*	30	*Pman*	53		
	l				*l*	*Pmc*2$_1$	26	*P*2*cm*	28	*Pmcm*	51
	l	*h*	*h*		*l*	*P*2$_1$*ca*	29	*Pmca*	57		
	l	*k*		*k*	*l*	*P*2*cb*	32	*Pmcb*	55		
	l	*h* + *k*	*h*	*k*	*l*	*P*2$_1$*cn*	33	*Pmcn*	62		
	h + *l*		*h*		*l*	*Pmn*2$_1$	31	*P*2$_1$*nm*	31	*Pmnm*	59
	h + *l*	*h*	*h*		*l*	*P*2*na*	30	*Pmna*	53		
	h + *l*	*k*	*h*	*k*	*l*	*P*2$_1$*nb*	33	*Pmnb*	62		
	h + *l*	*h* + *k*	*h*	*k*	*l*	*P*2*nn*	34	*Pmnn*	58		
k				*k*		*Pb*2$_1$*m*	26	*Pbm*2	28	*Pbmm*	51
k		*h*	*h*	*k*		*Pb*2$_1$*a*	29	*Pbma*	57		
k		*k*		*k*		*Pb*2*b*	27	*Pbmb*	49		
k		*h* + *k*	*h*	*k*		*Pb*2*n*	30	*Pbmn*	53		
k	*h*		*h*	*k*		*Pba*2	32	*Pbam*	55		
k	*h*	*h*	*h*	*k*		*Pbaa*	54				
k	*h*	*k*	*h*	*k*		*Pbab*	54				
k	*h*	*h* + *k*	*h*	*k*		*Pban*	50				
k	*l*			*k*	*l*	*Pbc*2$_1$	29	*Pbcm*	57		
k	*l*	*h*	*h*	*k*	*l*	*Pbca*	61				
k	*l*	*k*		*k*	*l*	*Pbcb*	54				
k	*l*	*h* + *k*	*h*	*k*	*l*	*Pbcn*	60				

Table 1.6.4.7 (continued)

Reflection conditions						Space group	No.	Space group	No.	Space group	No.
0*kl*	*h*0*l*	*hk*0	*h*00	0*k*0	00*l*						
k	*h* + *l*		*h*	*k*	*l*	*Pbn*2_1	33	*Pbnm*	62		
k	*h* + *l*	*h*	*h*	*k*	*l*	*Pbna*	60				
k	*h* + *l*	*k*	*h*	*k*	*l*	*Pbnb*	56				
k	*h* + *l*	*h* + *k*	*h*	*k*	*l*	*Pbnn*	52				
l					*l*	*Pcm*2_1	26	*Pc*2*m*	28	*Pcmm*	51
l		*h*	*h*		*l*	*Pc*2*a*	32	*Pcma*	55		
l		*k*		*k*	*l*	*Pc*2_1*b*	29	*Pcmb*	57		
l		*h* + *k*	*h*	*k*	*l*	*Pc*2_1*n*	33	*Pcmn*	62		
l	*h*		*h*		*l*	*Pca*2_1	29	*Pcam*	57		
l	*h*	*h*	*h*		*l*	*Pcaa*	54				
l	*h*	*k*	*h*	*k*	*l*	*Pcab*	61				
l	*h*	*h* + *k*	*h*	*k*	*l*	*Pcan*	60				
l	*l*				*l*	*Pcc*2	27	*Pccm*	49		
l	*l*	*h*	*h*		*l*	*Pcca*	54				
l	*l*	*k*		*k*	*l*	*Pccb*	54				
l	*l*	*h* + *k*	*h*	*k*	*l*	*Pccn*	56				
l	*h* + *l*		*h*		*l*	*Pcn*2	30	*Pcnm*	53		
l	*h* + *l*	*h*	*h*		*l*	*Pcna*	50				
l	*h* + *l*	*k*	*h*	*k*	*l*	*Pcnb*	60				
l	*h* + *l*	*h* + *k*	*h*	*k*	*l*	*Pcnn*	52				
k + *l*				*k*	*l*	*Pnm*2_1	31	*Pn*2_1*m*	31	*Pnmm*	59
k + *l*		*h*	*h*	*k*	*l*	*Pn*2_1*a*	33	*Pnma*	62		
k + *l*		*k*		*k*	*l*	*Pn*2*b*	30	*Pnmb*	53		
k + *l*		*h* + *k*	*h*	*k*	*l*	*Pn*2*n*	34	*Pnmn*	58		
k + *l*	*h*		*h*	*k*	*l*	*Pna*2_1	33	*Pnam*	62		
k + *l*	*h*	*h*	*h*	*k*	*l*	*Pnaa*	56				
k + *l*	*h*	*k*	*h*	*k*	*l*	*Pnab*	60				
k + *l*	*h*	*h* + *k*	*h*	*k*	*l*	*Pnan*	52				
k + *l*	*l*			*k*	*l*	*Pnc*2	30	*Pncm*	53		
k + *l*	*l*	*h*	*h*	*k*	*l*	*Pnca*	60				
k + *l*	*l*	*k*		*k*	*l*	*Pncb*	50				
k + *l*	*l*	*h* + *k*	*h*	*k*	*l*	*Pncn*	52				
k + *l*	*h* + *l*		*h*	*k*	*l*	*Pnn*2	34	*Pnnm*	58		
k + *l*	*h* + *l*	*h*	*h*	*k*	*l*	*Pnna*	52				
k + *l*	*h* + *l*	*k*	*h*	*k*	*l*	*Pnnb*	52				
k + *l*	*h* + *l*	*h* + *k*	*h*	*k*	*l*	*Pnnn*	48				

Table 1.6.4.8
Reflection conditions and possible space groups with Bravais lattice *oS* (*oC* setting) and Laue class *mmm*; Patterson symmetry *Cmmm*

Reflection conditions							Space group	No.	Space group	No.	Space group	No.
hkl	0*kl*	*h*0*l*	*hk*0	*h*00	0*k*0	00*l*						
$h + k$	k	h	$h + k$	h	k		***C*222** *C*2*mm*	21 38	*Cmm*2 *Cmmm*	35 65	*Cm*2*m*	38
$h + k$	k	h	$h + k$	h	k	l	***C*222$_1$**	20				
$h + k$	k	h	h, k	h	k		*Cm*2*e*	39	*C*2*me*	39	*Cme*	67
$h + k$	k	h, l	$h + k$	h	k	l	*Cmc*2$_1$	36	*C*2*cm*	40	*Cmcm*	63
$h + k$	k	h, l	h, k	h	k	l	*C*2*ce*	41	*Cmce*	64		
$h + k$	k, l	h	$h + k$	h	k	l	*Ccm*2$_1$	36	*Cc*2*m*	40	*Ccmm*	63
$h + k$	k, l	h	h, k	h	k	l	*Cc*2*e*	41	*Ccme*	64		
$h + k$	k, l	h, l	$h + k$	h	k	l	*Ccc*2	37	*Cccm*	66		
$h + k$	k, l	h, l	h, k	h	k	l	*Ccce*	68				

Table 1.6.4.9
Reflection conditions and possible space groups with Bravais lattice *oS* (*oB* setting) and Laue class *mmm*; Patterson symmetry *Bmmm*

Reflection conditions							Space group	No.	Space group	No.	Space group	No.
hkl	0*kl*	*h*0*l*	*hk*0	*h*00	0*k*0	00*l*						
$h + l$	l	$h + l$	h	h		l	***B*222** *B*2*mm*	21 38	*Bm*2*m* *Bmmm*	35 65	*Bmm*2	38
$h + l$	l	$h + l$	h	h	k	l	***B*22$_1$2**	20				
$h + l$	l	$h + l$	h, k	h	k	l	*Bm*2$_1$*b*	36	*B*2*mb*	40	*Bmmb*	63
$h + l$	l	h, l	h	h		l	*Bme*2	39	*B*2*em*	39	*Bmem*	67
$h + l$	l	h, l	h, k	h	k	l	*B*2*eb*	41	*Bmeb*	64		
$h + l$	k, l	$h + l$	h	h	k	l	*Bb*2$_1$*m*	36	*Bbm*2	40	*Bbmm*	63
$h + l$	k, l	$h + l$	h, k	h	k	l	*Bb*2*b*	37	*Bbmb*	66		
$h + l$	k, l	h, l	h	h	k	l	*Bbe*2	41	*Bbem*	64		
$h + l$	k, l	h, l	h, k	h	k	l	*Bbeb*	68				

Table 1.6.4.10
Reflection conditions and possible space groups with Bravais lattice *oS* (*oA* setting) and Laue class *mmm*; Patterson symmetry *Ammm*

Reflection conditions							Space group	No.	Space group	No.	Space group	No.
hkl	0*kl*	*h*0*l*	*hk*0	*h*00	0*k*0	00*l*						
$k + l$	$k + l$	l	k		k	l	***A*222** *Amm*2	21 38	*A*2*mm* *Ammm*	35 65	*Am*2*m*	38
$k + l$	$k + l$	l	k	h	k	l	***A*2$_1$22**	20				
$k + l$	$k + l$	l	h, k	h	k	l	*A*2$_1$*ma*	36	*Am*2*a*	40	*Amma*	63
$k + l$	$k + l$	h, l	k	h	k	l	*A*2$_1$*am*	36	*Ama*2	40	*Amam*	63
$k + l$	$k + l$	h, l	h, k	h	k	l	*A*2*aa*	37	*Amaa*	66		
$k + l$	k, l	l	k		k	l	*Aem*2	39	*Ae*2*m*	39	*Aemm*	67
$k + l$	k, l	l	h, k	h	k	l	*Ae*2*a*	41	*Aema*	64		
$k + l$	k, l	h, l	k	h	k	l	*Aea*2	41	*Aeam*	64		
$k + l$	k, l	h, l	h, k	h	k	l	*Aeaa*	68				

Table 1.6.4.11
Reflection conditions and possible space groups with Bravais lattice *oI* and Laue class *mmm*; Patterson symmetry *Immm*

Reflection conditions							Space group	No.	Space group	No.	Space group	No.
hkl	0*kl*	*h*0*l*	*hk*0	*h*00	0*k*0	00*l*						
$h+k+l$	$k+l$	$h+l$	$h+k$	h	k	l	***I*222** *Im*2*m*	23 44	$\boldsymbol{I2_12_12_1}$ *I*2*mm*	24 44	*Imm*2 *Immm*	44 71
$h+k+l$	$k+l$	$h+l$	h, k	h	k	l	*Im*2*a* *Immb*	46 74	*I*2*mb*	46	*Imma*	74
$h+k+l$	$k+l$	h, l	$h+k$	h	k	l	*Ima*2 *Imcm*	46 74	*I*2*cm*	46	*Imam*	74
$h+k+l$	$k+l$	h, l	h, k	h	k	l	*I*2*cb*	45	*Imcb*	72		
$h+k+l$	k, l	$h+l$	$h+k$	h	k	l	*Ibm*2 *Icmm*	46 74	*Ic*2*m*	46	*Ibmm*	74
$h+k+l$	k, l	$h+l$	h, k	h	k	l	*Ic*2*a*	45	*Icma*	72		
$h+k+l$	k, l	h, l	$h+k$	h	k	l	*Iba*2	45	*Ibam*	72		
$h+k+l$	k, l	h, l	h, k	h	k	l	*Ibca*	73	*Icab*	73		

Table 1.6.4.12
Reflection conditions and possible space groups with Bravais lattice *oF* and Laue class *mmm*; Patterson symmetry *Fmmm*

Reflection conditions							Space group	No.
hkl	0*kl*	*h*0*l*	*hk*0	*h*00	0*k*0	00*l*		
$h+k, h+l, k+l$	k, l	h, l	h, k	h	k	l	***F*222** *Fmm*2 *Fm*2*m* *F*2*mm* *Fmmm*	22 42 42 42 69
$h+k, h+l, k+l$	k, l	$h+l=4n; h, l$	$h+k=4n; h, k$	$h=4n$	$k=4n$	$l=4n$	*F*2*dd*	43
$h+k, h+l, k+l$	$k+l=4n; k, l$	h, l	$h+k=4n; h, k$	$h=4n$	$k=4n$	$l=4n$	*Fd*2*d*	43
$h+k, h+l, k+l$	$k+l=4n; k, l$	$h+l=4n; h, l$	h, k	$h=4n$	$k=4n$	$l=4n$	*Fdd*2	43
$h+k, h+l, k+l$	$k+l=4n; k, l$	$h+l=4n; h, l$	$h+k=4n; h, k$	$h=4n$	$k=4n$	$l=4n$	*Fddd*	70

Table 1.6.4.13
Reflection conditions and possible space groups with Bravais lattice *tP* and Laue class 4/*m*; *hk* are permutable; Patterson symmetry *P*4/*m*

Reflection conditions					Space group	No.	Space group	No.	Space group	No.
*hk*0	0*kl*	$h \pm h\, l$	00*l*	*h*00						
					***P*4**	75	$P\bar{4}$	81	$P4/m$	83
			l		$\boldsymbol{P4_2}$	77	$P4_2/m$	84		
			$l=4n$		$\boldsymbol{P4_1}$	76	$\boldsymbol{P4_3}$	78		
$h+k$				h	$P4/n$	85				
$h+k$			l	h	$P4_2/n$	86				

Table 1.6.4.14
Reflection conditions and possible space groups with Bravais lattice *tP* and Laue class 4/*mmm*; *hk* are permutable; Patterson symmetry *P*4/*mmm*

Reflection conditions					Space group	No.	Space group	No.	Space group	No.
*hk*0	0*kl*	*h* ± *h l*	00*l*	*h*00						
					***P*422**	89	*P*4*mm*	99	$P\bar{4}2m$	111
					$P\bar{4}m2$	115	*P*4/*mmm*	123		
				h	***P*42$_1$2**	90	$P\bar{4}2_1m$	113		
			l		***P*4$_2$22**	93				
			l	*h*	***P*4$_2$2$_1$2**	94				
			l = 4*n*		***P*4$_1$22**	91	***P*4$_3$22**	95		
			l = 4*n*	*h*	***P*4$_1$2$_1$2**	92	***P*4$_3$2$_1$2**	96		
		l	*l*		*P*4$_2$*mc*	105	$P\bar{4}2c$	112	*P*4$_2$/*mmc*	131
		l	*l*	*h*	$P\bar{4}2_1c$	114				
	k			*h*	*P*4*bm*	100	$P\bar{4}b2$	117	*P*4/*mbm*	127
	k	*l*	*l*	*h*	*P*4$_2$*bc*	106	*P*4$_2$/*mbc*	135		
	l		*l*		*P*4$_2$*cm*	101	$P\bar{4}c2$	116	*P*4$_2$/*mcm*	132
	l	*l*	*l*		*P*4*cc*	103	*P*4/*mcc*	124		
	k + *l*		*l*	*h*	*P*4$_2$*nm*	102	$P\bar{4}n2$	118	*P*4$_2$/*mnm*	136
	k + *l*	*l*	*l*	*h*	*P*4*nc*	104	*P*4/*mnc*	128		
h + *k*				*h*	*P*4/*nmm*	129				
h + *k*		*l*	*l*	*h*	*P*4$_2$/*nmc*	137				
h + *k*	*k*			*h*	*P*4/*nbm*	125				
h + *k*	*k*	*l*	*l*	*h*	*P*4$_2$/*nbc*	133				
h + *k*	*l*		*l*	*h*	*P*4$_2$/*ncm*	138				
h + *k*	*l*	*l*	*l*	*h*	*P*4/*ncc*	130				
h + *k*	*k* + *l*		*l*	*h*	*P*4$_2$/*nnm*	134				
h + *k*	*k* + *l*	*l*	*l*	*h*	*P*4/*nnc*	126				

Table 1.6.4.15
Reflection conditions and possible space groups with Bravais lattice *tI* and Laue class 4/*m*; *hk* are permutable; Patterson symmetry *I*4/*m*

Reflection conditions							Space group	No.	Space group	No.	Space group	No.
hkl	*hk*0	0*kl*	*h* ± *h l*	00*l*	*h*00	*h* ± *h* 0						
h + *k* + *l*	*h* + *k*	*k* + *l*	*l*	*l*	*h*		***I*4**	79	$I\bar{4}$	82	*I*4/*m*	87
h + *k* + *l*	*h* + *k*	*k* + *l*	*l*	*l* = 4*n*	*h*		***I*4$_1$**	80				
h + *k* + *l*	*h*, *k*	*k* + *l*	*l*	*l* = 4*n*	*h*	*h*	*I*4$_1$/*a*	88				

Table 1.6.4.16
Reflection conditions and possible space groups with Bravais lattice *tI* and Laue class 4/*mmm*; *hk* are permutable; Patterson symmetry *I*4/*mmm*

Reflection conditions							Space group	No.	Space group	No.	Space group	No.
hkl	*hk*0	0*kl*	$h \pm h\, l$	00*l*	*h*00	$h \pm h\, 0$						
$h+k+l$	$h+k$	$k+l$	l	l	h		**I422** $I\bar{4}2m$	97 121	$I4mm$ $I4/mmm$	107 139	$I\bar{4}m2$	119
$h+k+l$	$h+k$	$k+l$	l	$l=4n$	h		$\mathbf{I4_122}$	98				
$h+k+l$	$h+k$	$k+l$	$2h+l=4n$	$l=4n$	h	h	$I4_1md$	109	$I\bar{4}2d$	122		
$h+k+l$	$h+k$	k, l	l	l	h		$I4cm$	108	$I\bar{4}c2$	120	$I4/mcm$	140
$h+k+l$	$h+k$	k, l	$2h+l=4n$	$l=4n$	h	h	$I4_1cd$	110				
$h+k+l$	h, k	$k+l$	$2h+l=4n$	$l=4n$	h	h	$I4_1/amd$	141				
$h+k+l$	h, k	k, l	$2h+l=4n$	$l=4n$	h	h	$I4_1/acd$	142				

Table 1.6.4.17
Reflection conditions and possible space groups with Bravais lattice *hP* and Laue class $\bar{3}$; *hki* are permutable; Patterson symmetry $P\bar{3}$

Reflection conditions			Space group	No.	Space group	No.
$hh\bar{2}hl$	$h\bar{h}0l$	000*l*				
			P3	143	$P\bar{3}$	147
		$l=3n$	$\mathbf{P3_1}$	144	$\mathbf{P3_2}$	145

Table 1.6.4.18
Reflection conditions and possible space groups with Bravais lattice *hP* and Laue classes $\bar{3}1m$ and $\bar{3}m1$; *hki* are permutable; Patterson symmetry $P\bar{3}1m$ and $P\bar{3}m1$

Reflection conditions			Class $\bar{3}1m$		Class $\bar{3}m1$	
$hh\bar{2}hl$	$h\bar{h}0l$	000*l*	Space group	No.	Space group	No.
			P312	149	**P321**	150
			$P31m$	157	$P3m1$	156
			$P\bar{3}1m$	162	$P\bar{3}m1$	164
		$l=3n$	$\mathbf{P3_112}$	151	$\mathbf{P3_121}$	152
			$\mathbf{P3_212}$	153	$\mathbf{P3_221}$	154
l		l	$P31c$	159		
			$P\bar{3}1c$	163		
	l	l			$P3c1$	158
					$P\bar{3}c1$	165

Table 1.6.4.19
Reflection conditions and possible space groups with Bravais lattice *hP* and Laue class 6/*m*; *hki* are permutable; Patterson symmetry *P*6/*m*

Reflection conditions			Space group	No.	Space group	No.	Space group	No.
$hh\bar{2}hl$	$h\bar{h}0l$	000*l*						
			P6	168	$P\bar{6}$	174	$P6/m$	175
		l	$\mathbf{P6_3}$	173	$P6_3/m$	176		
		$l=3n$	$\mathbf{P6_2}$	171	$\mathbf{P6_4}$	172		
		$l=6n$	$\mathbf{P6_1}$	169	$\mathbf{P6_5}$	170		

Table 1.6.4.20
Reflection conditions and possible space groups with Bravais lattice *hP* and Laue class 6/*mmm*; *hki* are permutable; Patterson symmetry *P*6/*mmm*

Reflection conditions			Space group	No.	Space group	No.	Space group	No.
$hh\bar{2}\bar{h}l$	$h\bar{h}0l$	$000l$						
			***P*622**	177	*P*6*mm*	183	$P\bar{6}m2$	187
			$P\bar{6}2m$	189	*P*6/*mmm*	191		
		l	$\boldsymbol{P6_322}$	182				
		$l = 3n$	$\boldsymbol{P6_222}$	180	$\boldsymbol{P6_422}$	181		
		$l = 6n$	$\boldsymbol{P6_122}$	178	$\boldsymbol{P6_522}$	179		
l		l	$P6_3mc$	186	$P\bar{6}2c$	190	$P6_3/mmc$	194
	l	l	$P6_3cm$	185	$P\bar{6}c2$	188	$P6_3/mcm$	193
l	l	l	*P*6*cc*	184	*P*6/*mcc*	192		

Table 1.6.4.21
Reflection conditions and possible space groups with Bravais lattice *hR* and Laue class $\bar{3}$ (hexagonal axes); *hki* are permutable; Patterson symmetry $R\bar{3}$; Ov = obverse setting; Rv = reverse setting

Reflection conditions						Space group	No.	Space group	No.	
hkil	*hki*0	$hh\bar{2}\bar{h}l$	$h\bar{h}0l$	$000l$	$h\bar{h}00$					
$-h+k+l=3n$	$-h+k=3n$	$l=3n$	$h+l=3n$	$l=3n$	$h=3n$	***R*3**	146	$R\bar{3}$	148	Ov
$h-k+l=3n$	$h-k=3n$	$l=3n$	$-h+l=3n$	$l=3n$	$h=3n$	***R*3**	146	$R\bar{3}$	148	Rv

Table 1.6.4.22
Reflection conditions and possible space groups with Bravais lattice *hR* and Laue class $\bar{3}m$ (hexagonal axes); *hki* are permutable; Patterson symmetry $R\bar{3}m$; Ov = obverse setting; Rv = reverse setting

Reflection conditions						Space group	No.	Space group	No.	Space group	No.	
hkil	*hki*0	$hh\bar{2}\bar{h}l$	$h\bar{h}0l$	$000l$	$h\bar{h}00$							
$-h+k+l=3n$	$-h+k=3n$	$l=3n$	$h+l=3n$	$l=3n$	$h=3n$	***R*32**	155	*R*3*m*	160	$R\bar{3}m$	166	Ov
$-h+k+l=3n$	$-h+k=3n$	$l=3n$	$h+l=3n, l=2m$	$l=6n$	$h=3n$	*R*3*c*	161	$R\bar{3}c$	167			Ov
$h-k+l=3n$	$h-k=3n$	$l=3n$	$-h+l=3n$	$l=3n$	$h=3n$	***R*32**	155	*R*3*m*	160	$R\bar{3}m$	166	Rv
$h-k+l=3n$	$h-k=3n$	$l=3n$	$-h+l=3n, l=2m$	$l=6n$	$h=3n$	*R*3*c*	161	$R\bar{3}c$	167			Rv

Table 1.6.4.23
Reflection conditions and possible space groups with Bravais lattice *hR* and Laue class $\bar{3}$ (rhombohedral axes); *hkl* are permutable; Patterson symmetry $R\bar{3}$

Reflection conditions		Space group	No.	Space group	No.
hhl	*hhh*				
		***R*3**	146	$R\bar{3}$	148

Table 1.6.4.24
Reflection conditions and possible space groups with Bravais lattice *hR* and Laue class $\bar{3}m$ (rhombohedral axes); *hkl* are permutable; Patterson symmetry $R\bar{3}m$

Reflection conditions		Space group	No.	Space group	No.	Space group	No.
hhl	*hhh*						
		***R*32**	155	*R*3*m*	160	$R\bar{3}m$	166
l	h	*R*3*c*	161	$R\bar{3}c$	167		

Table 1.6.4.25
Reflection conditions and possible space groups with Bravais lattice *cP* and Laue class $m\bar{3}$; *hkl* are cyclically permutable; Patterson symmetry $Pm\bar{3}$

Reflection conditions			Space group	No.	Space group	No.
$0kl$	$h \pm h\,l$	$h00$				
			***P*23**	195	$Pm\bar{3}$	200
		h	***P*2$_1$3**	198		
k		h	$Pa\bar{3}$	205		
l		h	$Pb\bar{3}$	205		
$k + l$		h	$Pn\bar{3}$	201		

Table 1.6.4.26
Reflection conditions and possible space groups with Bravais lattice *cP* and Laue class $m\bar{3}m$; *hkl* are permutable; Patterson symmetry $Pm\bar{3}m$

Reflection conditions			Space group	No.	Space group	No.	Space group	No.
$0kl$	$h \pm h\,l$	$h00$						
			***P*432**	207	$P\bar{4}3m$	215	$Pm\bar{3}m$	221
		h	***P*4$_2$32**	208				
		$h = 4n$	***P*4$_3$32**	212	***P*4$_1$32**	213		
	l	h	$P\bar{4}3n$	218	$Pm\bar{3}n$	223		
$k + l$		h	$Pn\bar{3}m$	224				
$k + l$	l	h	$Pn\bar{3}n$	222				

Table 1.6.4.27
Reflection conditions and possible space groups with Bravais lattice *cI* and Laue class $m\bar{3}$; *hkl* are cyclically permutable; Patterson symmetry $Im\bar{3}$

Reflection conditions				Space group	No.	Space group	No.	Space group	No.
hkl	$0kl$	$h \pm h\,l$	$h00$						
$h + k + l$	$k + l$	l	h	***I*23**	197	***I*2$_1$3**	199	$Im\bar{3}$	204
$h + k + l$	k, l	l	h	$Ia\bar{3}$	206				

Table 1.6.4.28
Reflection conditions and possible space groups with Bravais lattice *cI* and Laue class $m\bar{3}m$; *hkl* are permutable; Patterson symmetry $Im\bar{3}m$

Reflection conditions				Space group	No.	Space group	No.	Space group	No.
hkl	$0kl$	$h \pm h\,l$	$h00$						
$h + k + l$	$k + l$	l	h	***I*432**	211	$I\bar{4}3m$	217	$Im\bar{3}m$	229
$h + k + l$	$k + l$	l	$h = 4n$	***I*4$_1$32**	214				
$h + k + l$	$k + l$	$2h + l = 4n$	$h = 4n$	$I\bar{4}3d$	220				
$h + k + l$	k, l	$2h + l = 4n$	$h = 4n$	$Ia\bar{3}d$	230				

Table 1.6.4.29
Reflection conditions and possible space groups with Bravais lattice *cF* and Laue class $m\bar{3}$; *hkl* are cyclically permutable; Patterson symmetry $Fm\bar{3}$

Reflection conditions				Space group	No.	Space group	No.
hkl	$0kl$	$h \pm h\,l$	$h00$				
$h + k, h + l, k + l$	k, l	$h + l$	h	***F*23**	196	$Fm\bar{3}$	202
$h + k, h + l, k + l$	$k + l = 4n; k, l$	$h + l$	$h = 4n$	$Fd\bar{3}$	203		

Table 1.6.4.30
Reflection conditions and possible space groups with Bravais lattice *cF* and Laue class $m\bar{3}m$; *hkl* are permutable; Patterson symmetry $Fm\bar{3}m$

Reflection conditions				Space group	No.	Space group	No.	Space group	No.
hkl	0*kl*	$h \pm hl$	*h*00						
$h+k, h+l, k+l$	k, l	$h+l$	h	***F*432**	209	$F\bar{4}3m$	216	$Fm\bar{3}m$	225
$h+k, h+l, k+l$	k, l	$h+l$	$h=4n$	***F*4$_1$32**	210				
$h+k, h+l, k+l$	k, l	h, l	h	$F\bar{4}3c$	219	$Fm\bar{3}c$	226		
$h+k, h+l, k+l$	$k+l=4n; k, l$	$h+l$	$h=4n$	$Fd\bar{3}m$	227				
$h+k, h+l, k+l$	$k+l=4n; k, l$	h, l	$h=4n$	$Fd\bar{3}c$	228				

and have not yet enjoyed widespread distribution, use and acceptance by the community. Flack *et al.* (2011) and Parsons *et al.* (2012) give detailed information on these calculations.

1.6.5.1.2. Status of centrosymmetry and resonant scattering

The basic starting point in this analysis is the following linear transformation of $|F(hkl)|^2$ and $|F(\overline{hkl})|^2$, applicable to both observed and model values, to give the average (A) and difference (D) intensities:

$$A(hkl) = \tfrac{1}{2}[|F(hkl)|^2 + |F(\overline{hkl})|^2],$$
$$D(hkl) = |F(hkl)|^2 - |F(\overline{hkl})|^2.$$

In equation (1.6.2.1), $A(hkl)$ was denoted by $|F_{\rm av}(hkl)|^2$. The expression for $D(hkl)$ corresponding to that for $A(hkl)$ given in equation (1.6.2.1) and using the same nomenclature is

$$D(\mathbf{h}) = \sum_{i,j}[(f_i + f_i')f_j'' - (f_j + f_j')f_i'']\sin[2\pi\mathbf{h}(\boldsymbol{r}_i - \boldsymbol{r}_j)].$$

In general $|D(hkl)|$ is small compared to $A(hkl)$. A compound with an appreciable resonant-scattering contribution has $|D(hkl)| \approx 0.01A(hkl)$, whereas a compound with a small resonant-scattering contribution has $|D(hkl)| \approx 0.0001A(hkl)$. For centric reflections, $D_{\rm model} = 0$, and so the values of $D_{\rm obs}(hkl)$ of these are entirely due to random uncertainties and systematic errors in the intensity measurements. $D_{\rm obs}(hkl)$ of acentric reflections contains contributions both from the random uncertainties and the systematic errors of the data measurements, and from the differences between $|F(hkl)|^2$ and $|F(\overline{hkl})|^2$ which arise through the effect of resonant scattering. A slight experimental limitation is that a data set of intensities needs to contain both reflections *hkl* and $\overline{hkl}$ in order to obtain $A_{\rm obs}(hkl)$ and $D_{\rm obs}(hkl)$.

The Bijvoet ratio, defined by

$$\chi = \frac{\langle D^2\rangle^{1/2}}{\langle A\rangle},$$

is the ratio of the root-mean-square value of D to the mean value of A. In a structure analysis, two independent estimates of the Bijvoet ratio are available and their comparison leads to useful information as to whether the crystal structure is centrosymmetric or not.

The first estimate arises from considerations of intensity statistics leading to the definition of the Bijvoet ratio as a value called Friedif$_{\rm stat}$, whose functional form was derived by Flack & Shmueli (2007) and Shmueli & Flack (2009). One needs only to know the chemical composition of the compound and the wavelength of the X-radiation to calculate Friedif$_{\rm stat}$ using various available software.

The second estimate of the Bijvoet ratio, Friedif$_{\rm obs}$, is obtained from the observed diffraction intensities. One problematic point in the evaluation of Friedif$_{\rm obs}$ arises because A and D do not have the same dependence on $\sin\theta/\lambda$ and it is necessary to eliminate this difference as far as possible. A second problematic point in the calculation is to make sure that only acentric reflections of any of the noncentrosymmetric point groups in the chosen Laue class are selected for the calculation of Friedif$_{\rm obs}$. In this way one is sure that if the point group of the crystal is centrosymmetric, all of the chosen reflections are centric, and if the point group of the crystal is noncentrosymmetric, all of the chosen reflections are acentric. The necessary selection is achieved by taking only those reflections that are general in the Laue group. To date (2015), the calculation of Friedif$_{\rm obs}$ is not available in distributed software. On comparison of Friedif$_{\rm stat}$ with Friedif$_{\rm obs}$, one is able to state with some confidence that:

(1) if Friedif$_{\rm obs}$ is much lower than Friedif$_{\rm stat}$, then the crystal structure is either centrosymmetric, and random uncertainties and systematic errors in the data set are minor, or noncentrosymmetric with the crystal twinned by inversion in a proportion close to 50:50;
(2) if Friedif$_{\rm obs}$ is close in value to Friedif$_{\rm stat}$, then the crystal is probably noncentrosymmetric and random uncertainties and systematic errors in the data set are minor. However, data from a centrosymmetric crystal with large random uncertainties and systematic errors may also produce this result; and
(3) if Friedif$_{\rm obs}$ is much larger than Friedif$_{\rm stat}$ then either the data set is dominated by random uncertainties and systematic errors or the chemical formula is erroneous.

Example 1

The crystal of compound Ex1 (Udupa & Krebs, 1979) is known to be centrosymmetric (space group $P2_1/c$) and has a significant resonant-scattering contribution, Friedif$_{\rm stat}$ = 498 and Friedif$_{\rm obs}$ = 164. The comparison of Friedif$_{\rm stat}$ and Friedif$_{\rm obs}$ indicates that the crystal structure is centrosymmetric.

Example 2

The crystal of compound Ex2, potassium hydrogen (2*R*,3*R*) tartrate, is known to be enantiomerically pure and appears in space group $P2_12_12_1$. The value of Friedif$_{\rm obs}$ is 217 compared to a Friedif$_{\rm stat}$ value of 174. The agreement is good and allows the deduction that the crystal is neither centrosymmetric, nor twinned by inversion in a proportion near to 50:50, nor that the

Table 1.6.5.1
R_{merge} values for Ex2 for the 589 sets of general reflections of *mmm* which have all eight measurements in the set

R_{merge} (%)	*mmm*	2*mm*	*m*2*m*	*mm*2	222
R_A	1.30	1.30	1.30	1.30	1.30
R_D	100.0	254.4	235.7	258.1	82.9

Table 1.6.5.2
R_{merge} values for Ex1 for the 724 sets of general reflections of 2/*m* which have all four measurements in the set

R_{merge} (%)	2/*m*	*m*	2
R_A	1.29	1.29	1.29
R_D	100.0	98.3	101.7

data set is unsatisfactorily dominated by random uncertainty and systematic error.

Example 3

The crystals of compound Ex3 (Zhu & Jiang, 2007) occur in Laue group $\overline{1}$. One finds Friedif_{stat} = 70 and Friedif_{obs} = 499. The huge discrepency between the two shows that the observed values of D are dominated by random uncertainty and systematic error.

1.6.5.1.3. Resolution of noncentrosymmetric ambiguities

It was shown in Section 1.6.5.1.2 that under certain circumstances it is possible to determine whether or not the space group of the crystal investigated is centrosymmetric. Suppose that the space group was found to be noncentrosymmetric. In each Laue class, there is one centrosymmetric point group and one or more noncentrosymmetric point groups. For example, in the Laue class *mmm* we need to distinguish between the point groups 222, 2*mm*, *m*2*m* and *mm*2, and of course between the space groups based on them. We shall show that it is possible in practice to distinguish between these noncentrosymmetric point groups using intensity differences between Friedel opposites caused by resonant scattering.

An excellent intensity data set from a crystal (Ex2 above) of potassium hydrogen (2*R*, 3*R*) tartrate, measured with a wavelength of 0.7469 Å at 100 K, was used. The Laue group was assumed to be *mmm*. The raw data set was initially merged and averaged in point group 1 and all special reflections of the Laue group *mmm* (*i.e.* 0*kl*, *h*0*l*, *hk*0, *h*00, 0*k*0, 00*l*) were set aside. The remaining data were organized into sets of reflections symmetry-equivalent under the Laue group *mmm*, and only those sets (589 in all) containing all 8 of the *mmm*-symmetry-equivalent reflections were retained. Each of these sets provides 4 A_{obs} and 4 D_{obs} values which can be used to calculate R_{merge} values appropriate to the five point groups in the Laue class *mmm*. The results are given in Table 1.6.5.1. The value of 100% for R_{merge} in a centrosymmetric point group, such as *mmm* or 2/*m*, arises by definition and not by coincidence. The R_D of the true point group has the lowest value, which is noticeably different from the other choices of point group.

The crystal of Ex1 above (space group $P2_1/c$) was treated in a similar manner. Table 1.6.5.2 shows that R_D values display no preference between the three point groups in Laue class 2/*m*.

Intensity measurements comprising a full sphere of reflections are essential to the success of the R_{merge} tests described in this section.

1.6.5.1.4. Data evaluation after structure refinement

There is an excellent way in which to evaluate both data measurement and treatment procedures, and the fit of the model to the data, including the space-group assignment, at the completion of structure refinement. This technique is applicable both to noncentrosymmetric and to centrosymmetric crystals. A scattergram of D_{obs} against D_{model}, and $2A_{obs}$ against $2A_{model}$ pairs are plotted on the same graph. All (D_{obs}, D_{model}) pairs are plotted together with those ($2A_{obs}$, $2A_{model}$) pairs which have $2A_{obs} < |D_{obs}|_{max}$. The range of values on the axes of the model and of the observed values should be identical. For acentric reflections, for both A and D, a good fit of the observed to the model quantities shows itself as a straight line of slope 1 passing through the origin, with some scatter about this ideal straight line. For an individual reflection, 2A and D are, respectively, the sum and the difference of the same quantities and they have identical standard uncertainties. It is thus natural to select 2A and D to plot on the same graph. In practice one sees that the spread of the 2A plot increases with increasing value of 2A. Fig. 1.6.5.1 shows the 2AD plot for Ex2 of Example 2 in Section 1.6.5.1.2, which is most satisfactory and confirms the choice of point group from the use of R_{merge}. The conventional R value for all reflections is 3.1% and for those shown in Fig. 1.6.5.1 it is 10.4%. The R value for all D values is good at 51.1%. Fig. 1.6.5.2 shows the 2AD plot for Ex1 of Example 1 in Section 1.6.5.1.2. The structure model is centrosymmetric so all D_{model} values are zero. The conventional R value on A for all reflections is 4.3% and for those shown in Fig. 1.6.5.2 it is 9.1%. The R value on all the D values is 100%.

1.6.5.2. Space-group determination in macromolecular crystallography

For macromolecular crystallography, succinct descriptions of space-group determination have been given by Kabsch (2010*a*,*b*, 2012) and Evans (2006, 2011). Two characteristics of macromolecular crystals give rise to variations on the small-molecule procedures described above.

The first characteristic is the large size of the unit cell of macromolecular crystals and the variation of the cell dimensions from one crystal to another. This makes the determination of the Bravais lattice by cell reduction problematic, as small changes of cell dimensions give rise to differences in the assignment. Kabsch (2010*a*,*b*, 2012) uses a 'quality index' from each of Niggli's 44 lattice characters to come to a best choice. Grosse-Kunstleve *et al.* (2004) and Sauter *et al.* (2004) have found that some commonly used methods to determine the Bravais lattice are susceptible to numerical instability, making it possible for high-symmetry Bravais lattice types to be improperly identified. Sauter *et al.* (2004, 2006) find from practical experience that a deviation δ as high as 1.4° from perfect alignment of direct and reciprocal lattice rows must be allowed to construct the highest-symmetry Bravais type consistent with the data. Evans (2006) uses a value of 3.0°. The large unit-cell size also gives rise to a large number of reflections in the asymmetric region of reciprocal space, and taken with the tendency of macromolecular crystals to decompose in the X-ray beam, full-sphere data sets are uncommon. This means that confirmation of the Laue class by means of values of R_{int} (R_{merge}) are rarer than with small-molecule crystallography, although Kabsch (2010*b*) does use a 'redundancy-independent R factor'. Evans (2006, 2011) describes methods very similar to those given as the second stage in Section 1.6.2.1. The conclusion of Sauter *et al.* (2006) and Evans (2006) is that R_{int} values as high

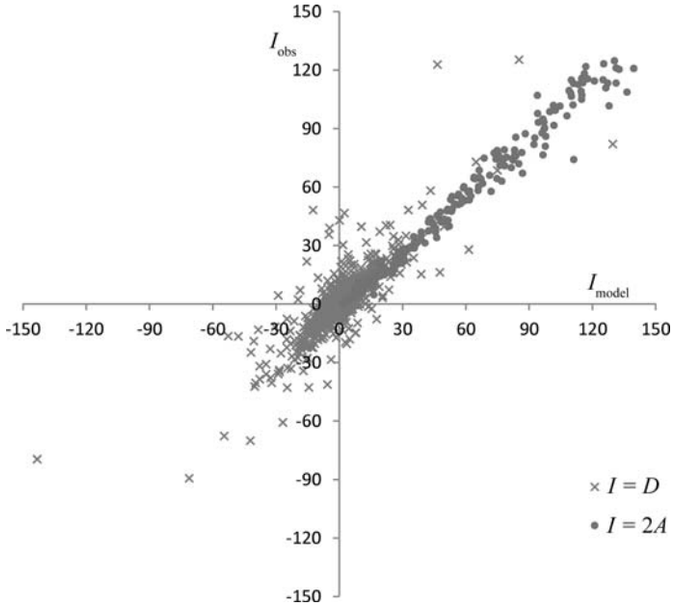

Figure 1.6.5.1
Data-evaluation plot for crystal Ex2. The plot shows a scattergram of all (D_{obs}, D_{model}) pairs and those ($2A_{obs}$, $2A_{model}$) pairs in the same intensity range as the D values.

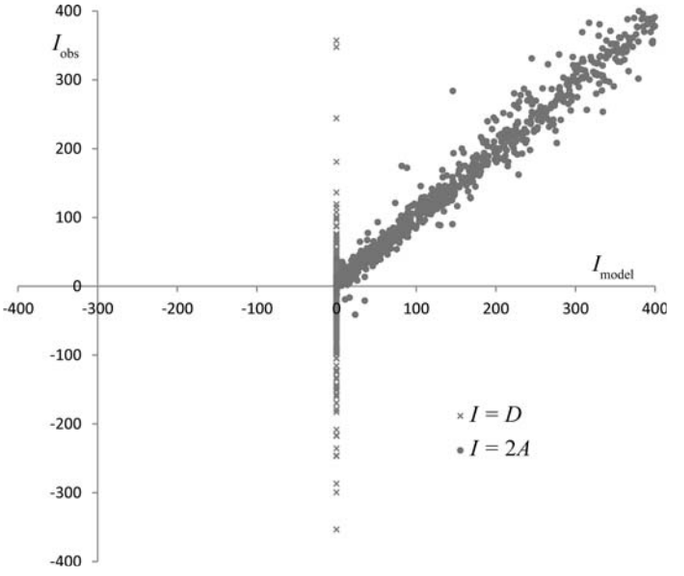

Figure 1.6.5.2
Data-evaluation plot for crystal Ex1. The plot shows a scattergram of all (D_{obs}, D_{model}) and some ($2A_{obs}$, $2A_{model}$) data points.

as 25% must be permitted in order to assemble an optimal set of operations to describe the diffraction symmetry. Another interesting procedure, accompanied by experimental proof, has been devised by Sauter *et al.* (2006). They show that it is clearer to calculate R_{merge} values individually for each potential symmetry operation of a target point group rather than comparing R_{merge} values for target point groups globally. According to Sauter *et al.* (2006) the reason for this improvement lies in the lack of intensity data relating some target symmetry operations.

The second characteristic of macromolecular crystals is that the compound is known, or presumed, to be chiral and enantiomerically pure, so that the crystal structure is chiral. This limits the choice of space group to the 65 Sohncke space groups containing only translations, pure rotations or screw rotations. For ease of use, these have been typeset in bold in Tables 1.6.4.2–1.6.4.30.

For the evaluation of protein structures, Poon *et al.* (2010) apply similar techniques to those described in Section 1.6.2.3. The major tactical objective is to identify pairs of α-helices that have been declared to be symmetry-independent in the structure solution but which may well be related by a rotational symmetry of the crystal structure. Poon *et al.* (2010) have been careful to test their methodology against generated structural data before proceeding to tests on real data. Their results indicate that some 2% of X-ray structures in the Protein Data Bank potentially fit in a higher-symmetry space group. Zwart *et al.* (2008) have studied the problems of under-assigned translational symmetry operations, suspected incorrect symmetry and twinned data with ambiguous space-group choices, and give illustrations of the uses of group–subgroup relations.

1.6.5.3. Space-group determination from powder diffraction

In powder diffraction, the reciprocal lattice is projected onto a single dimension. This projection gives rise to the major difficulty in interpreting powder-diffraction patterns. Reflections overlap each other either exactly, owing to the symmetry of the lattice metric, or approximately. This makes the extraction of the integrated intensities of individual Bragg reflections liable to error. Experimentally, the use of synchrotron radiation with its exceedingly fine and highly monochromatic beam has enabled considerable progress to be made over recent years. Other obstacles to the interpretation of powder-diffraction patterns, which occur at all stages of the analysis, are background interpretation, preferred orientation, pseudo-translational symmetry and impurity phases. These are general powder-diffraction problems and will not be treated at all in the current chapter. The reader should consult David *et al.* (2002) and David & Shankland (2008) or the forthcoming new volume of *International Tables for Crystallography* (Volume H, *Powder Diffraction*) for further information.

It goes without saying that the main use of the powder method is in structural studies of compounds for which single crystals cannot be grown.

Let us start by running through the three stages of extraction of symmetry information from the diffraction pattern described in Section 1.6.2.1 to see how they apply to powder diffraction.

(1) Stage 1 concerns the determination of the Bravais lattice from the experimentally determined cell dimensions. As such, this process is identical to that described in Section 1.6.2.1. The obstacle, arising from peak overlap, is the initial indexing of the powder pattern and the determination of a unit cell, see David *et al.* (2002) and David & Shankland (2008).

(2) Stage 2 concerns the determination of the point-group symmetry of the intensities of the Bragg reflections. As a preparation to stages 2 and 3, the integrated Bragg intensities have to be extracted from the powder-diffraction pattern by one of the commonly used profile analysis techniques [see David *et al.* (2002) and David & Shankland (2008)]. The intensities of severely overlapped reflections are subject to error. Moreover, the exact overlap of reflections owing to the symmetry of the lattice metric makes it impossible to distinguish between high- and low-symmetry Laue groups in the same family *e.g.* between 4/*m* and 4/*mmm* in the tetragonal family and $m\bar{3}$ and $m\bar{3}m$ in the cubic family. Likewise,

differences in intensity between Friedel opposites, *hkl* and $\overline{hkl}$, are hidden in a powder-diffraction pattern and the techniques of Section 1.6.5.1 are inapplicable. It is also known that experimental results on structure-factor statistics described in Section 1.6.2.2 are sensitive to the algorithm used to extract the integrated Bragg intensities from the powder-diffraction pattern. One procedure tends to produce intensity statistics typical of the noncentrosymmetric space group $P1$ and another those of the centrosymmetric space group $P\overline{1}$. In all, nothing much can be learnt from stage 2 for a powder-diffraction pattern. As a consequence, space-group determination from powder diffraction relies entirely on the Bravais lattice derived from the indexing of the diffraction pattern in stage 1 and the detection of systematic absences in stage 3.

(3) Stage 3 concerns the identification of the conditions for possible systematic absences. However, Bragg-peak overlap causes difficulties with determining systematic absences. For powder-diffraction peaks at small values of $\sin\theta/\lambda$, the problem is rarely severe, even for low-resolution laboratory powder-diffraction data. Potentially absent reflections at higher values of $\sin\theta/\lambda$ often overlap with other reflections of observable intensity. Accordingly, conclusions about the presence of space-group symmetry operations are generally drawn on the basis of a very small number of clear intensity observations. Observing lattice-centring absences is usually relatively easy. In the case of molecular organic materials, considerable help in space-group selection comes from the well known frequency distribution of space groups, where some 80% of compounds crystallize in one of the following: $P2_1/c$, $P\overline{1}$, $P2_12_12_1$, $P2_1$ and $C2/c$. Practical methods of proceeding are described by David & Sivia (2002). It should also be pointed out that Table 1.6.4.1 in this chapter may often be found to be helpful. For example, if it is known that the Bravais lattice is of type *cP*, Table 1.6.4.1 tells us that the possible Laue classes are $m\overline{3}$ and $m\overline{3}m$ and the possible space groups can be found in Tables 1.6.4.25 and 1.6.4.26, respectively. The appropriate reflection conditions are of course given in these tables. All relevant tables can thus be located with the aid of Table 1.6.4.1 if the Bravais lattice is known.

There has been considerable progress since 2000 in the automated extraction by software of the set of conditions for reflections from a powder-diffraction pattern for undertaking stage 3 above. Once the conditions have been identified, Tables 1.6.4.2–1.6.4.30 are used to identify the corresponding space groups. The output of such software consists of a ranked list of complete sets of conditions for reflections (*i.e.* the horizontal rows of conditions given in Tables 1.6.4.2–1.6.4.30). Accordingly, the best-ranked set of conditions is at the top of the list followed by others in decreasing order of appropriateness. The list thus is answering the question: Which is the most probable set of reflection conditions for the data to hand? Such software uses integrated intensities of Bragg reflections extracted from the powder pattern and, as mentioned above, the results are sensitive to the particular profile integration procedure used. Moreover, only ideal Wilson (1949) p.d.f.'s for space groups $P1$ and $P\overline{1}$ are implemented. The art of such techniques is to find appropriate criteria such that the most likely set of reflection conditions is clearly discriminated from any others. Altomare *et al.* (Altomare, Caliandro, Camalli, Cuocci, da Silva *et al.*, 2004; Altomare, Caliandro, Camalli, Cuocci, Giacovazzo *et al.*, 2004; Altomare *et al.*, 2005, 2007, 2009) have used a probabilistic approach combining the probabilities of individual symmetry operations of candidate space groups. The approach is pragmatic and has evolved over several versions of the software. Experience has accumulated through use of the procedure and the discrimination of the software has consequently improved. Markvardsen *et al.* (2001, 2012) commence with an in-depth probabilistic analysis using the concepts of Bayesian statistics which was demonstrated on a few test structures. Later, Markvardsen *et al.* (2008) made software generally available for their approach. Vallcorba *et al.* (2012) have also produced software for space-group determination, but give little information on their algorithm.

1.6.6. Space groups for nanocrystals by electron microscopy

By J. C. H. Spence

The determination of crystal space groups may be achieved by the method of convergent-beam electron microdiffraction (CBED) using a modern transmission electron microscope (TEM). A detailed description of the CBED technique is given by Tanaka (2008) in Section 2.5.3 of Volume B; here we give a brief overview of the capabilities of the method for space-group determination, for completeness. A TEM beam focused to nanometre dimensions allows study of nanocrystals, while identification of noncentrosymmetric crystals is straightforward, as a result of the strong multiple scattering normally present in electron diffraction. (Unlike single scattering, this does not impose inversion symmetry on diffraction patterns, but preserves the symmetry of the sample and its boundaries.) CBED patterns also allow direct determination of screw and glide space-group elements, which produce characteristic absences, despite the presence of multiple scattering, in certain orientations. These absences, which remain for all sample thicknesses and beam energies, may be shown to occur as a result of an elegant cancellation theorem along symmetry-related multiple-scattering paths (Gjønnes & Moodie, 1965). Using all of the above information, most of the 230 space groups can be distinguished by CBED. The remaining more difficult cases (such as space groups that differ only in the location of their symmetry elements) are discussed in Spence & Lynch (1982), Eades (1988), and Saitoh *et al.* (2001). Enantiomorphic pairs require detailed atomistic simulations based on a model, as in the case of quartz (Goodman & Secomb, 1977). Multiple scattering renders Bragg intensities sensitive to structure-factor phases in noncentrosymmetric structures, allowing these to be measured with a tenth of a degree accuracy (Zuo *et al.*, 1993). Unlike X-ray diffraction, electron diffraction is very sensitive to ionicity and bonding effects, especially at low angles, allowing extinction-free charge-density mapping with high accuracy (Zuo, 2004; Zuo *et al.*, 1999). Because of its sensitivity to strain, CBED may also be used to map out local phase transformations which cause space-group changes on the nanoscale (Zuo, 1993; Zhang *et al.*, 2006).

In simplest terms, a CBED pattern is formed by enlarging the incident beam divergence in the transmission diffraction geometry, as first demonstrated G. Mollenstedt in 1937 (Kossel & Mollenstedt, 1942). Bragg spots are then enlarged into discs, and the intensity variation within these discs is studied, in addition to that of the entire pattern, in the CBED method. The intensity variation within a disc displays a complete rocking curve in each of the many diffracted orders, which are simultaneously excited

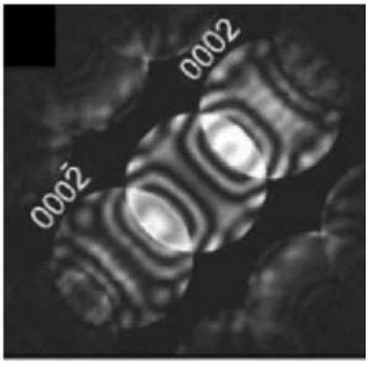

Figure 1.6.6.1
Polarity determination by convergent-beam electron diffraction. A CBED pattern from ZnO with the beam normal to the *c* axis is shown. The intensity distribution along **c** does not have inversion symmetry, reflecting the noncentrocentrosymmetric nature of the structure. Reproduced with permission from Wang *et al.* (2003). Copyright (2003) by The American Physical Society.

and recorded. The entire pattern thus consists of many independent 'point' diffraction patterns (each for a slightly different incident beam direction) laid beside each other. Fig. 1.6.6.1 shows a CBED pattern from the wurtzite structure of ZnO, with the beam normal to the *c* axis (Wang *et al.*, 2003). The intensity variation along a line running through the centres of these discs (along the *c* axis) is not an even function, strongly violating Friedel's law for this elastic scattering. At higher scattering angles, curvature of the Ewald sphere allows three-dimensional symmetry elements to be determinated by taking account of 'out-of-zone' intensities in the outer higher-order Laue zone (HOLZ) rings near the edge of the detector. Since sub-ångstrom-diameter electron probes and nanometre X-ray laser probes (Spence *et al.*, 2012) are now being used, the effect of the inevitable coherent interference between overlapping convergent-beam orders on space-group determination must be considered (Spence & Zuo, 1992).

A systematic approach to space-group determination by CBED has been developed by several groups. In general, one would determine the symmetry of the projection diffraction group first (ignoring diffraction components along the beam direction *z*), then add the *z*-dependent information seen in HOLZ lines, allowing one to finally identify the point group from tables, by combining all this information. After indexing the pattern, in order to determine a unit cell the Bravais lattice is next determined. The form of the three-dimensional reciprocal lattice and its centring can usually be determined by noting the registry of Bragg spots in a HOLZ ring against those in the zero-order (ZOLZ) ring. Finally, by setting up certain special orientations, tests are applied for the presence of screw and glide elements, which are revealed by a characteristic dark line or cross within the CBED discs. Tables can again then be used to combine these translational symmetry elements with the previously determined point group, to find the space group. As a general experimental strategy, one first seeks mirror lines (perhaps seen in Kikuchi patterns), then follows these around using the two-axis goniometer fitted to modern TEM instruments in a systematic search for other symmetry elements. Reviews of the CBED method can be found in Steeds & Vincent (1983), in Goodman (1975), and in the texts by Tanaka *et al.* (1988). A textbook-level worked example of space-group determination by CBED can be found in Spence & Zuo (1992) and in the chapter by A. Eades in Williams & Carter (2009).

References

Allenmark, S., Gawronski, J. & Berova, N. (2007). Editors. *Chirality*, **20**, 605–759.

Altomare, A., Caliandro, R., Camalli, M., Cuocci, C., da Silva, I., Giacovazzo, C., Moliterni, A. G. G. & Spagna, R. (2004). *Space-group determination from powder diffraction data: a probabilistic approach*. *J. Appl. Cryst.* **37**, 957–966.

Altomare, A., Caliandro, R., Camalli, M., Cuocci, C., Giacovazzo, C., Moliterni, A. G. G. & Rizzi, R. (2004). *Automatic structure determination from powder data with EXPO2004*. *J. Appl. Cryst.* **37**, 1025–1028.

Altomare, A., Camalli, M., Cuocci, C., da Silva, I., Giacovazzo, C., Moliterni, A. G. G. & Rizzi, R. (2005). *Space group determination: improvements in EXPO2004*. *J. Appl. Cryst.* **38**, 760–767.

Altomare, A., Camalli, M., Cuocci, C., Giacovazzo, C., Moliterni, A. G. G. & Rizzi, R. (2007). *Advances in space-group determination from powder diffraction data*. *J. Appl. Cryst.* **40**, 743–748.

Altomare, A., Camalli, M., Cuocci, C., Giacovazzo, C., Moliterni, A. & Rizzi, R. (2009). *EXPO2009: structure solution by powder data in direct and reciprocal space*. *J. Appl. Cryst.* **42**, 1197–1202.

Authier, A., Borovik-Romanov, A. S., Boulanger, B., Cox, K. G., Dmitrienko, V. E., Ephraïm, M., Glazer, A. M., Grimmer, H., Janner, A., Jannsen, T., Kenzelmann, M., Kirfel, A., Kuhs, W. F., Küppers, H., Mahan, G. D., Ovchinnikova, E. N., Thiers, A., Zarembowitch, A. & Zyss, J. (2014). *International Tables for Crystallography*, Volume D, *Physical Properties of Crystals*, edited by A. Authier, 2nd edition, Part 1. Chichester: Wiley.

Boček, P., Hahn, Th., Janovec, V., Klapper, H., Kopský, V., Přivratska, J., Scott, J. F. & Tolédano, J.-C. (2014). *International Tables for Crystallography*, Volume D, *Physical Properties of Crystals*, edited by A. Authier, 2nd ed., Part 3. Chichester: Wiley.

Buerger, M. J. (1935). *The application of plane groups to the interpretation of Weissenberg photographs*. *Z. Kristallogr.* **91**, 255–289.

Buerger, M. J. (1942). *X-ray Crystallography*, ch. 22. New York: Wiley.

Buerger, M. J. (1946). *The interpretation of Harker syntheses*. *J. Appl. Phys.* **17**, 579–595.

Buerger, M. J. (1969). *Diffraction symbols*. In *Physics of the Solid State*, edited by S. Balakrishna, ch. 3, pp. 27–42. London: Academic Press.

Burzlaff, H., Zimmermann, H. & de Wolff, P. M. (2002). *Crystal lattices*. In *International Tables for Crystallography*, Volume A, *Space-Group Symmetry*, edited by Th. Hahn, 5th ed., Part 9. Dordrecht: Kluwer Academic Publishers.

David, W. I. F. & Shankland, K. (2008). *Structure determination from powder diffraction data*. *Acta Cryst.* A**64**, 52–64.

David, W. I. F., Shankland, K., McCusker, L. B. & Baerlocher, Ch. (2002). Editors. *Structure Determination from Powder Diffraction Data*. IUCr Monograph No. 13. Oxford University Press.

David, W. I. F. & Sivia, D. S. (2002). *Extracting integrated intensities from powder diffraction patterns*. In *Structure Determination from Powder Diffraction Data*, edited by W. I. F. David, K. Shankland, L. B. McCusker & Ch. Baerlocher. IUCr Monograph No. 13. Oxford University Press.

Eades, J. A. (1988). *Glide planes and screw axes in CBED*. In *Microbeam Analysis 1988*, edited by D. Newberry, pp. 75–78. San Francisco Press.

Evans, P. (2006). *Scaling and assessment of data quality*. *Acta Cryst.* D**62**, 72–82.

Evans, P. R. (2011). *An introduction to data reduction: space-group determination, scaling and intensity statistics*. *Acta Cryst.* D**67**, 282–292.

Flack, H. D. (2003). *Chiral and achiral crystal structures*. *Helv. Chim. Acta*, **86**, 905–921.

Flack, H. D. (2015). *Methods of space-group determination – a supplement dealing with twinned crystals and metric specialization*. *Acta Cryst.* C**71**, 916–920.

Flack, H. D., Sadki, M., Thompson, A. L. & Watkin, D. J. (2011). *Practical applications of averages and differences of Friedel opposites*. *Acta Cryst.* A**67**, 21–34.

Flack, H. D. & Shmueli, U. (2007). *The mean-square Friedel intensity difference in P1 with a centrosymmetric substructure*. *Acta Cryst.* A**63**, 257–265.

Giacovazzo, C. (2008). *Direct methods*. In *International Tables for Crystallography*, Volume B, *Reciprocal Space*, edited by U. Shmueli, ch. 2.2, pp. 215–243. Dordrecht: Springer.

Gjønnes, J. & Moodie, A. F. (1965). *Extinction conditions in the dynamic theory of electron diffraction*. *Acta Cryst.* **19**, 65–69.

Goodman, P. (1975). *A practical method of three-dimensional space-group analysis using convergent-beam electron diffraction*. *Acta Cryst.* A**31**, 804–810.

Goodman, P. & Secomb, T. W. (1977). *Identification of enantiomorphously related space groups by electron diffraction*. *Acta Cryst.* A**33**, 126–133.

Grosse-Kunstleve, R. W., Sauter, N. K. & Adams, P. D. (2004). *Numerically stable algorithms for the computation of reduced unit cells*. *Acta Cryst.* A**60**, 1–6.

Howells, E. R., Phillips, D. C. & Rogers, D. (1950). *The probability distribution of X-ray intensities. II. Experimental investigation and the X-ray detection of centres of symmetry*. *Acta Cryst.* **3**, 210–214.

Kabsch, W. (2010*a*). *XDS*. *Acta Cryst.* D**66**, 125–132.

Kabsch, W. (2010*b*). *Integration, scaling, space-group assignment and post-refinement*. *Acta Cryst.* D**66**, 133–144.

Kabsch, W. (2012). *Space-group assignment*. In *International Tables for Crystallography*, Volume F, *Crystallography of Biological Macromolecules*, edited by E. Arnold, D. M. Himmel & M. G. Rossmann, Section 11.3.6. Chichester: Wiley.

Kirschbaum, K., Martin, A. & Pinkerton, A. A. (1997). *λ/2 Contamination in charge-coupled-device area-detector data*. *J. Appl. Cryst.* **30**, 514–516.

Koch, E. (2006). *Twinning*. In *International Tables for Crystallography*, Volume C, *Mathematical, Physical and Chemical Tables*, 1st online edition, edited by E. Prince, ch. 1.3. Chester: International Union of Crystallography.

Kossel, W. & Mollenstedt, G. (1942). *Electron interference in a convergent beam*. *Ann. Phys.* **42**, 287–296.

Le Page, Y. (1982). *The derivation of the axes of the conventional unit cell from the dimensions of the Buerger-reduced cell*. *J. Appl. Cryst.* **15**, 255–259.

Le Page, Y. (1987). *Computer derivation of the symmetry elements implied in a structure description*. *J. Appl. Cryst.* **20**, 264–269.

Looijenga-Vos, A. & Buerger, M. J. (2002). *Space-group determination and diffraction symbols*. In *International Tables for Crystallography*, Volume A, *Space-Group Symmetry*, 5th ed., edited by Th. Hahn, Section 3.1.3. Dordrecht, Boston, London: Kluwer Academic Publishers.

Macchi, P., Proserpio, D. M., Sironi, A., Soave, R. & Destro, R. (1998). *A test of the suitability of CCD area detectors for accurate electron-density studies*. *J. Appl. Cryst.* **31**, 583–588.

Markvardsen, A. J., David, W. I. F., Johnson, J. C. & Shankland, K. (2001). *A probabilistic approach to space-group determination from powder data*. *Acta Cryst.* A**57**, 47–54.

Markvardsen, A. J., David, W. I. F., Johnston, J. C. & Shankland, K. (2012). *A probabilistic approach to space-group determination from powder data. Corrigendum*. *Acta Cryst.* A**68**, 780.

Markvardsen, A. J., Shankland, K., David, W. I. F., Johnston, J. C., Ibberson, R. M., Tucker, M., Nowell, H. & Griffin, T. (2008). *ExtSym: a program to aid space-group determination from powder diffraction data*. *J. Appl. Cryst.* **41**, 1177–1181.

Nespolo, M., Ferraris, G. & Souvignier, B. (2014). *Effects of merohedric twinning on the diffraction pattern*. *Acta Cryst.* A**70**, 106–125.

Okaya, Y. & Pepinsky, R. (1955). *Computing Methods and the Phase Problem in X-ray Crystal Analysis*, p. 276. Oxford: Pergamon Press.

Oszlányi, G. & Sütő, A. (2004). *Ab initio structure solution by charge flipping*. *Acta Cryst.* A**60**, 134–141.

Palatinus, L. (2011). Private communication.

Palatinus, L. & van der Lee, A. (2008). *Symmetry determination following structure solution in P1*. *J. Appl. Cryst.* **41**, 975–984.

Parsons, S., Pattison, P. & Flack, H. D. (2012). *Analyzing Friedel averages and differences*. *Acta Cryst.* A**68**, 736–749.

Poon, B. K., Grosse-Kunstleve, R. W., Zwart, P. H. & Sauter, N. K. (2010). *Detection and correction of underassigned rotational symmetry prior to structure deposition*. *Acta Cryst.* D**66**, 503–513.

Rabinovich, S., Shmueli, U., Stein, Z., Shashua, R. & Weiss, G. H. (1991). *Exact random-walk models in crystallographic statistics. VI. P.d.f.'s of E for all plane groups and most space groups*. *Acta Cryst.* A**47**, 328–335.

Rogers, D. (1950). *The probability distribution of X-ray intensities. IV. New methods of determining crystal classes and space groups*. *Acta Cryst.* **3**, 455–464.

Rossmann, M. G. & Arnold, E. (2001). *Patterson and molecular replacement techniques*. In *International Tables for Crystallography*, Volume B, *Reciprocal Space*, edited by U. Shmueli, ch. 2.3, pp. 235–263. Dordrecht: Kluwer Academic Publishers.

Saitoh, K., Tsuda, K., Terauchi, M. & Tanaka, M. (2001). *Distinction between space groups having principal rotation and screw axes, which are combined with twofold rotation axes, using the coherent convergent-beam electron diffraction method*. *Acta Cryst.* A**57**, 219–230.

Sauter, N. K., Grosse-Kunstleve, R. W. & Adams, P. D. (2004). *Robust indexing for automatic data collection*. *J. Appl. Cryst.* **37**, 399–409.

Sauter, N. K., Grosse-Kunstleve, R. W. & Adams, P. D. (2006). *Improved statistics for determining the Patterson symmetry from unmerged diffraction intensities*. *J. Appl. Cryst.* **39**, 158–168.

Shmueli, U. (2007). *Theories and Techniques of Crystal Structure Determination*. Oxford University Press.

Shmueli, U. (2008). *Symmetry in reciprocal space*. In *International Tables for Crystallography*, Volume B, *Reciprocal Space*, edited by U. Shmueli, 3rd ed., ch. 1.4, Appendix A1.4.4. Dordrecht: Springer.

Shmueli, U. (2012). *Structure-factor statistics and crystal symmetry*. *J. Appl. Cryst.* **45**, 389–392.

Shmueli, U. (2013). *INSTAT: a program for computing non-ideal probability density functions of |E|*. *J. Appl. Cryst.* **46**, 1521–1522.

Shmueli, U. & Flack, H. D. (2009). *Concise intensity statistics of Friedel opposites and classification of the reflections*. *Acta Cryst.* A**65**, 322–325.

Shmueli, U. & Weiss, G. H. (1995). *Introduction to Crystallographic Statistics*. Oxford University Press.

Shmueli, U., Weiss, G. H., Kiefer, J. E. & Wilson, A. J. C. (1984). *Exact random-walk models in crystallographic statistics. I. Space groups $P\bar{1}$ and P1*. *Acta Cryst.* A**40**, 651–660.

Shmueli, U. & Wilson, A. J. C. (2008). *Statistical properties of the weighted reciprocal lattice*. In *International Tables for Crystallography*, Volume B, *Reciprocal Space*, edited by U. Shmueli, ch. 2.1. Dordrecht: Springer.

Spek, A. L. (2003). *Single-crystal structure validation with the program PLATON*. *J. Appl. Cryst.* **36**, 7–13.

Spence, J. C. H. & Lynch, J. (1982). *Stem microanalysis by transmission electron energy loss spectroscopy in crystals*. *Ultramicroscopy*, **9**, 267–276.

Spence, J. C. H., Weierstall, U. & Chapman, H. (2012). *X-ray lasers for structural biology*. *Rep. Prog. Phys.* **75**, 102601.

Spence, J. & Zuo, J. M. (1992). *Electron Microdiffraction*. New York: Plenum.

Steeds, J. W. & Vincent, R. (1983). *Use of high-symmetry zone axes in electron diffraction in determining crystal point and space groups*. *J. Appl. Cryst.* **16**, 317–325.

Tadbuppa, P. P. & Tiekink, E. R. T. (2010). *[(Z)-Ethyl N-isopropylthiocarbamato-κS](tricyclohexylphosphine-κP)gold(I)*. *Acta Cryst.* E**66**, m615.

Tanaka, M. (2008). *Point-group and space-group determination by convergent-beam electron diffraction*. In *International Tables for Crystallography*, Volume B, *Reciprocal Space*, edited by U. Shmueli, 3rd ed., Section 2.5.3. Springer.

Tanaka, M., Terauchi, M. & Kaneyama, T. (1988). *Convergent Beam Electron Diffraction* (and subsequent volumes in the same series). Tokyo: JEOL Ltd.

Udupa, M. R. & Krebs, B. (1979). *Crystal and molecular structure of creatininium tetrachlorocuprate(II)*. *Inorg. Chim. Acta*, **33**, 241–244.

Vallcorba, O., Rius, J., Frontera, C., Peral, I. & Miravitlles, C. (2012). *DAJUST: a suite of computer programs for pattern matching, space-group determination and intensity extraction from powder diffraction data*. *J. Appl. Cryst.* **45**, 844–848.

Wang, Z. L., Kong, X. Y. & Zuo, J. M. (2003). *Induced growth of asymmetric nanocantilever on polar surfaces*. *Phys. Rev. Lett.* **91**, 185502.

Waser, J. (1955). *Symmetry relations between structure factors*. *Acta Cryst.* **8**, 595.

Wells, M. (1965). *Computational aspects of space-group symmetry*. *Acta Cryst.* **19**, 173–179.

Williams, D. & Carter, C. B. (2009). *Transmission Electron Microscopy*, ch. 6. New York: Springer.

Wilson, A. J. C. (1949). *The probability distribution of X-ray intensities*. *Acta Cryst.* **2**, 318–321.

Zhang, P., Kisielowski, C., Istratov, A., He, H., Nelson, C., Mardinly, J., Weber, E. & Spence, J. C. H. (2006). *Direct strain measurement in a*

65 nm node strained silicon transistor by convergent-beam electron diffraction. *Appl. Phys. Lett.* **89**, 161907.
Zhu, H.-Y. & Jiang, S.-D. (2007). *1,3,4,6-Tetra-O-acetyl-2-(trifluoromethylsulfonyl)-β-*D*-mannopyranose*. *Acta Cryst.* E**63**, o2833.
Zuo, J. M. (1993). *New method of Bravais lattice determination*. *Ultramicroscopy*, **52**, 459–464.
Zuo, J. M. (2004). *Measurements of electron densities in solids: a real-space view of electronic structure and bonding in inorganic crystals*. *Rep. Prog. Phys.* **67**, 2053–2129.
Zuo, J. M., Kim, M., O'Keeffe, M. & Spence, J. C. H. (1999). *Observation of d holes and Cu-Cu bonding in cuprite*. *Nature (London)*, **401**, 49–52.
Zuo, J. M., Spence, J. C. H., Downs, J. & Mayer, J. (1993). *Measurement of individual structure-factor phases with tenth-degree accuracy: the 00.2 reflection in BeO studied by electron and X-ray diffraction*. *Acta Cryst.* A**49**, 422–429.
Zwart, P. H., Grosse-Kunstleve, R. W., Lebedev, A. A., Murshudov, G. N. & Adams, P. D. (2008). *Surprises and pitfalls from (pseudo)symmetry*. *Acta Cryst.* D**64**, 99–107.